Graphene nanoplatelet-modified epoxy: Effect of aspect ratio and surface functionality on mechanical properties and toughening mechanisms

H. M. Chong[a,c], S. J. Hinder[b], A. C. Taylor[a,*]

[a] *Department of Mechanical Engineering, Imperial College London, South Kensington Campus, London SW7 2AZ, UK*
[b] *The Surface Analysis Laboratory, Faculty of Engineering and Physical Sciences, University of Surrey, Guildford, Surrey GU2 7XH, UK*
[c] *Present address: Singapore Institute of Manufacturing Technology, 71 Nanyang Drive, 638075, Singapore*

Abstract

Graphene has the potential to act as a high-performance reinforcement for adhesives or fibre composites when combined with epoxy polymer. However, it is currently mostly available not as single high aspect ratio sheets but as graphene nanoplatelets (GNPs), comprised of stacks of graphene sheets. Graphene nanoplatelets of a range of lateral size, thickness, aspect ratio and surface functionality were used to modify an anhydride cured epoxy polymer. The morphology, mechanical properties and toughening mechanisms of these modified epoxies were investigated. The GNPs were sonicated in tetrahydrofuran (THF) or n-methyl-pyrrolidone (NMP) to facilitate dispersion in the epoxy. The use of THF resulted in large agglomerates, whereas more finely dispersed stacks of GNPs were observed for NMP. The maximum values of modulus (3.6 GPa at 1 wt%) and fracture energy (343 J/m^2 at 2 wt%) were

*Corresponding author, Tel.: +44 20 7594 7149
Email address: a.c.taylor@imperial.ac.uk (A. C. Taylor)

measured for the epoxy modified with an intermediate platelet size of approximately 4 μm, compared to 2.9 GPa and 96 J/m^2 respectively for the unmodified epoxy. The Young's modulus was highly dependent on the dispersion quality, whereas the fracture energy was independent of the degree of GNP dispersion. The larger agglomerates of the GNPs which were dispersed in THF toughened the epoxy by crack deflection, whereas the GNPs dispersed in NMP showed platelet debonding, pull-out and plastic void growth of the epoxy. This work indicates that reinforcement and toughening can be achieved at much lower contents than for conventional modifiers. Further, achieving a good dispersion is crucial to the engineering application of these materials, and intermediate-sized graphene achieves the best balance of properties.

Keywords: nanocomposites, polymers, fracture

---

1. Introduction

Epoxy polymers have good engineering properties that make them attractive for use in applications such as structural adhesives or as the matrix of fibre composites. However, these highly crosslinked thermosetting polymers have low fracture toughness. The modification of these brittle materials by the addition of particles into the polymer or into the matrix of fibre composites is an effective method to improve the fracture toughness and has been studied in detail for the past few decades [1, 2].

Graphene has extremely high stiffness and strength, and when combined with polymers has shown promising functional properties such as conductivity (e.g. [3, 4]). Hence graphene has the potential to be a highly effective

multifunctional reinforcement. However, the transfer of the high stiffness and strength of graphene to reinforce a polymer is difficult to achieve due to the problems in dispersing graphene and achieving strong platelet-matrix interfacial adhesion. Detailed reviews on graphene research have been published [5, 6], specifically regarding its use as polymer reinforcement. The majority of the early research was based on graphene oxide [7–10], which can be easily exfoliated and dispersed in epoxy due to the attached functional groups. However, these functional groups reduce the mechanical properties and their weight causes wrinkling of the graphene sheets [11]. Graphene nanoplatelets (GNPs) have been proposed as a lower cost option relative to carbon nanotubes and single layer graphene, providing conductivity at a very low particle content whilst providing reinforcement and toughening that cannot be achieved using carbon black. GNPs are small stacks of multiple graphene sheets, typically derived from bulk graphite compounds. Recent studies on the use of graphene in the form of graphene nanoplatelets [12–14] have shown some positive results. However the mechanisms involved are not well understood, and in general only a single type is studied, rather than comparing GNPs from several sources to understand how the particle geometry and surface chemistry influence the properties, as has been done in the present work.

One of the first publications concerning the mechanical properties of GNP modified epoxy by Rafiee *et al.* [13] compared GNPs to carbon nanotubes (CNTs). At the low weight percentages used, they showed that GNPs were more effective at increasing the modulus and fracture toughness than CNTs. However, they did not report on the quality of dispersion. Chatterjee *et al.*

[12] concluded that GNPs with a larger lateral dimension toughen epoxies more effectively, but did not report on the aspect ratios and dispersion quality. Additionally, only two micrometre scale GNPs were tested. Zaman *et al.* [15] incorporated GNPs into two epoxy polymers, one with a high glass transition temperature, T_g, and one with a low T_g, and found higher values of fracture toughness for the high T_g epoxy system. The authors claimed this was due to better compatibility between the epoxy and GNP, as well as better dispersion, in the high T_g system. However, this was not clearly presented and compared in their scanning electron microscope (SEM) images. In a separate study, they modified the GNPs with methylene diphenyl diisocyanate (MDI) to increase the interfacial adhesion between the GNPs and the epoxy [14]. Although a higher fracture toughness was measured for the surface modified GNPs, the Young's modulus decreased. This indicates a weaker interfacial strength and also resulted in more agglomerated GNPs, as evident in their transmission electron microscope (TEM) micrographs.

The purpose of the present study is to investigate how the properties of GNPs affect the mechanical and fracture performance of a typical epoxy polymer. An anhydride cured epoxy was used, into which GNPs of varying lateral size, thickness, aspect ratio and surface functionality were added. The bulk GNPs were characterised, and the morphology, mechanical properties and toughening mechanisms of the GNP modified epoxies were evaluated. The tensile and fracture properties were also compared with analytical models based on the physically observed mechanisms. Combining knowledge of the toughening and reinforcement mechanisms of GNPs with their known conductivity will enable the development of truly multifunctional thermoset

polymers for adhesives or fibre composites for aerospace and automotive applications.

2. Experimental

2.1. Materials

An anhydride cured diglycidyl ether of bisphenol A (DGEBA) epoxy was used. The epoxy resin was a standard DGEBA epoxy with an epoxide equivalent weight (EEW) of 185 g/eq, 'Araldite LY556' from Huntsman, UK. The curing agent was an accelerated methylhexahydrophthalic acid anhydride with an anhydride equivalent weight (AEW) of 170 g/eq, 'Albidur HE600' from Evonik Hanse, Germany. The epoxy resin and curing agent were used at stoichiometric quantities.

The graphene nanoplatelets (GNP) used in this study are summarised in Table 1. In total, six types of graphene nanoplatelets and one graphite flake modifier were used.

The graphene nanoplatelets from XG Sciences and Graphene Supermarket were manufactured from acid intercalated natural crystalline graphite flakes. Three grades of GNPs from XG Sciences were used, which vary in lateral size and thickness. During manufacturing, the graphite intercalation compounds were exfoliated by heating rapidly to 900°C using microwaves. When heated, the acid vaporises and forces the layers apart. The exfoliated graphite sheets were then pulverised into nanoplatelets by ultrasonic agitation in acetone [22]. The graphene nanoplatelets from Haydale, UK, were produced using a "split plasma" process. The GNPs produced from graphite intercalate compounds use strong acids that can damage the mate-

Table 1: Graphene nanoplatelet and graphite flake modifiers used in this study. Values quoted are from manufacturer data sheets [16–21].

Supplier	**Product name**	**Abbreviation**	**Thickness (nm)**	**Average lateral size (μm)**
XG Sciences, USA	xGnP-C-750	XG-C	2	2
	xGnP-H-5	XG-H	11 - 15	5
	xGnP-M-25	XG-M	6	25
Graphene Supermarket, USA	Graphene nanopowder flakes	GS	12	1.5 - 10
Haydale, UK	GNP-COOH	GNP-COOH	< 50	0.3 - 5
	GNP-O_2	GNP-O_2	< 50	0.3 - 5
Alfa Aesar, UK	Graphite flake	GF	> 100	70 - 100

rial structure and require a drying process downstream. The "split plasma" process is a low temperature, less aggressive process which does not damage the material surface and structure. The GNPs were functionalised by plasma treatment in oxygen or acid vapour by the manufacturers.

2.2. Bulk material

The GNP modifiers were supplied as dry powders, which had to be dispersed into the epoxy resin. The modifiers were first dispersed by ultrasonication using a Cole-Parmer CPX 750 ultrasonic probe in tetrahydrofuran (THF) or n-methyl-pyrrolidone (NMP) for a total of 20 min. The solvents were from Sigma-Aldrich, UK, and were used as received. The ultrasonic probe was used at a power of 225 W and a frequency of 20 kHz. The epoxy resin was then added into the modifier/solvent mixture and sonicated for a

further 10 min. The solvent was subsequently removed by stirring and heating above the solvent's boiling point (90°C for THF and 220°C for NMP). Alternatively, the functionalised GNPs (GNP-COOH and GNP-O2) were sonicated directly into the epoxy resin for 30 min. Next, the mixture was degassed in a vacuum oven at 60°C and monitored by weighing the mixture at 30 minute intervals to ensure that all of the solvent was removed.

The curing agent was added and stirred thoroughly at 60°C and at 200 rpm for 15 min using a 'RZR 2012' mechanical stirrer from Heidolph, Germany. The mixture was then degassed at 60°C in a vacuum oven. The epoxy resins were cast into preheated steel vertical moulds which had been coated with release agent ('Frekote 55NC' from Henkel, UK) to produce epoxy plates of 3 mm and 6 mm thickness. The moulds were then placed in a fan oven, and the epoxy was cured at 90°C for 60 min, followed by a post-cure at 160°C for 120 min.

The various types of GNPs will be labelled as per the abbreviations in Table 1, followed by the solvent used to initially disperse the GNPs (either THF or NMP), e.g. XG-H-NMP for the XG-H GNPs dispersed in NMP. In the Figures, the GNPs dispersed in THF are represented by a solid point and line, and the GNPs dispersed in NMP by an open point and dotted line.

To test the effects of residual solvents on the unmodified epoxy polymers, 10 wt% of each solvent was added to the unmodified epoxy polymer. This is roughly equivalent to the amount used to disperse the GNPs. For one set of results, the solvents were evaporated as per the method described and another set was made without removing the solvent.

2.3. GNP characterisation

The d-spacing and crystal size of the GNPs were characterised by X-ray diffraction (XRD) using an X'Pert Pro multi-purpose diffractometer, from PANalytical, Netherlands, fitted with a PW3064/60 diffractometer and X'Celerator detector. The samples were placed on a powder sample tray and exposed to Cu Kα X-ray radiation, which has a characteristic wavelength of 1.540598 Å. The X-rays were generated from the Cu anode at a generator voltage of 40 kV and tube current of 40 mA. Continuous scans were collected over a range of 2θ from 5 to 60° with a step size of 0.02° and dwell time of 20 s per step. Quantitative analysis was conducted using the accompanying software, PANalytical High Score Plus. The distance between individual platelets (d-spacing) was calculated using Bragg's Law and the positions of the *00l* peaks were used to calculate the d-spacing of the GNPs in bulk. The GNPs are multi-layer graphitic materials rather than single layer graphene, hence only the peaks from *002* and above are observed. The crystal size, L, is related to the thickness of the platelets and can be calculated using the Scherrer equation [23].

The particle sizes of the bulk GNPs were measured using laser light scattering (LLS) using a ZetaPALS Zeta Potential Analyser, from Brookhaven, USA. A 35 mW red diode laser with a wavelength of 660 nm was used and the results were averaged over 10 runs. The platelets were dispersed in distilled water by sonicating for 30 min. The results are given as the differential distribution, $G(d)$ of the intensity of scattered light at each value of diameter. The effective diameters were taken as the 95th percentile of the differential distribution of the intensity of the scattered light.

The surface chemical compositions of the GNPs were determined using X-ray photoelectron spectroscopy (XPS). XPS analyses were performed on a ThermoFisher Scientific Instruments (East Grinstead, UK) Theta Probe spectrometer. The instrument had a base operating pressure of 10^{-9} mbar. An MXR1 monochromatic Al Kα X-ray source, with a photon energy of 1486.6 eV, was used for all acquisitions. An X-ray spot size of 400 μm diameter was employed. All Survey spectra were acquired with a Pass Energy of 300 eV, a step size of 0.4 eV and 3 scans. The high resolution, core level spectra for C1s were acquired using a Pass Energy of 20 eV, a step size of 0.2 eV and 20 scans. The high resolution, core level spectra for O1s, Si2p and S2p were acquired using a Pass Energy of 50 eV, a step size of 0.2 eV and 20 scans. The high resolution, core level spectra of N1s and F1s were acquired with a Pass Energy of 100 eV, a 0.2 eV step size and 20 scans. Quantitative surface chemical compositions were determined from the high resolution, core level spectra following the removal of a non-linear (Shirley) background. The manufacturer's Avantage software was used which incorporates the appropriate sensitivity factors and corrects for the electron energy analyser transmission function. The transmission function corrects for the detection efficiency of the spectrometer, which is a function of the electron kinetic energy and can vary with the Pass Energy [24]. The GNP powder samples were fixed to the sample stage with double sided adhesive tape.

2.4. Dynamic mechanical analysis

The glass transition temperature (T_{g}) of each of the bulk samples was measured using dynamic mechanical analysis (DMA), using a Q800 from TA

Instruments, UK. Samples of dimensions 60 × 10 × 3 mm^3 were tested in double cantilever mode at 1 Hz. A temperature range of -100 to 200°C and a heating rate of 2°C/min were used. The storage modulus, loss modulus and tan δ were calculated as a function of temperature, where the T_{g} was defined as the temperature corresponding to the peak tan δ value.

2.5. Mechanical tests

Uniaxial tensile tests were performed to obtain the Young's modulus and tensile yield stress according to the ISO 527 [25] test standard. The tests were performed with dumb-bell shaped test specimens of type 1BA, machined from 3 mm thick bulk plates using a router. A gauge length of 25 mm and displacement rate of 1 mm/min were used. The tests were performed using an Instron 3392 universal testing machine and the displacement was measured with an Instron 2620-601 dynamic extensometer attached to the sample during testing. At least 5 samples were tested for each formulation.

Plane strain compression (PSC) tests were conducted to determine the compressive yield stress and yield behaviour, as described by Williams and Ford [26]. Test specimens of size 40 × 40 × 3 mm^3 were loaded in compression between two parallel dies of 12 mm width at a displacement rate of 0.1 mm/min using an Instron 5585H universal testing machine. The results were then corrected for machine and test rig compliance by compressing the two dies together with no sample and subtracting the resulting extensions from the results. At least 2 samples were tested for each formulation.

The PSC sample surfaces were polished with 4000 grit sandpaper using a LaboPol-21 polishing machine from Struers, Denmark. The contact surfaces were lubricated to further reduce friction using 'BRZ plus multi-grease EP

grease' from Dow Corning, UK. The true compressive stress, σ_c, and true compressive strain, ε_c, were calculated as [26]:

$$\sigma_c = \left(\frac{\sqrt{3}}{2}\right)\sigma_E \tag{1}$$

$$\varepsilon_c = \left(\frac{2}{\sqrt{3}}\right)\ln\left(\frac{B_\mathrm{C}}{B}\right) \tag{2}$$

where σ_E is the engineering stress, B_C is the compressed thickness and B is the initial thickness. The yield behaviour of glassy polymers is highly dependent on the hydrostatic pressure [27]. However, the tensile yield stress, σ_{yt} can be related to the compressive yield stress, σ_{yc}, by the relationship [28]:

$$\sigma_{yt} = \sigma_{yc}\frac{3^{1/2} - \mu_m}{3^{1/2} + \mu_m} \tag{3}$$

where μ_m is a material constant, usually taken as 0.2 [29].

A cross-section from each formulation which had been loaded to the strain softening region was examined by cross-polarised light microscopy. The samples were first cut with a Struers Accutom-5 precision cutter, equipped with a 10S15 silicon carbide cut-off wheel, polished, and mounted on glass microscopy slides with an optically transparent adhesive, 'Araldite 2020' from Huntsman, UK. The samples were then ground to a thickness of 100 μm and polished before being examined.

2.6. Fracture tests

Single edge notched bending (SENB) tests were conducted to determine the fracture toughness (K_C) and fracture energy (G_C) of the materials according to ISO 13586 [30]. Test specimens with a size of 60 × 12 × 6 mm^3

were cut from the bulk plates, and then notched 4 mm deep using a horizontal mill. A sharp crack of length $a/W \approx 0.5$ was then initiated by tapping a liquid nitrogen chilled razor blade into the notch, where a is the crack length and W is the width. The tests were performed on an Instron 3392 universal testing machine at a constant displacement rate of 1 mm/min under three-point bending. The displacement was measured with an Instron 2620-601 dynamic extensometer and at least 6 samples were tested for each formulation. The crack lengths were measured post-test using a Nikon SMZ800 optical microscope. The value of G_{C} was calculated using the energy method [30], and the value of K_{C} was calculated using the fracture load.

2.7. Fractography

A Carl Zeiss Leo 1525 field-emission gun scanning electron microscope (FEGSEM) was used to obtain high-resolution images of the GNPs and fracture surfaces. The bulk GNPs were adhered to an aluminium stub using conductive tape. For the fracture surfaces, the samples were first cut shorter using a Struers Accutom-5 precision cutter equipped with a saw blade. The samples were then sputter-coated with an approximately 5-nm thick layer of chromium to prevent charging. An accelerating voltage of 5 kV and a typical working distance of 6-8 mm were used for the microscopic observation.

3. Results and discussion

3.1. Particle size analysis

The X-ray diffraction patterns are shown in Figure 1 for the XG-H, XG-M, XG-C, GS, GNP-COOH and GNP-O_2 GNPs. The position of the *002*

peaks for all of the GNPs correspond well to those of bulk graphite, typically at $2\theta = 26.7°$ [31]. The differences in peak height (intensity) between each sample are irrelevant because they are dependent on sample preparation. The sharpness of the peaks also clearly indicate that the GNPs have a crystalline structure. The full width at half maximum (FWHM) values for all the GNPs, except for the XG-C GNP, were below 0.7°. The XG-C GNPs have a higher FWHM value of 1.67°, which indicates stacking defects and disorder in the crystal structure.

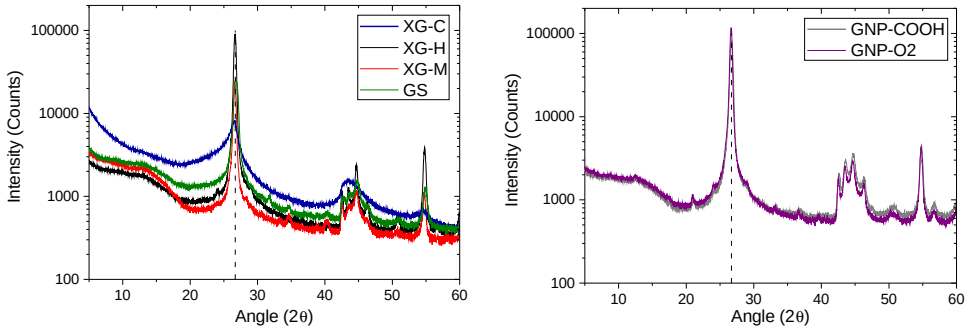

Figure 1: X-ray diffraction patterns obtained for bulk graphene nanoplatelets. The black dotted lines represent the locations of the *002* peaks.

The d-spacing and crystal sizes calculated from the XRD analysis are summarised in Table 2. The d-spacing was measured to be approximately 0.334 nm for all the GNPs, which is similar to graphite and indicates that the processing methods have removed the acid intercalant in the XG-H, XG-M, XG-C and GS GNPs. The crystal size in this case is related to the thickness of the GNPs. The calculated values of crystal size for the XG-C, GS, GNP-COOH and GNP-O_2 show good agreement with the values of thickness from the manufacturers, as shown in Table 2. However, the thickness of the XG-H

and XG-M GNPs were larger than expected, at 31.1 and 28.8 nm respectively, which suggests a lower aspect ratio for these samples than the manufacturer's data.

Table 2: d-spacing, full width half maximum (FWHM) of *002* peak and crystal size measurements from X-ray diffraction.

Modifier	d-spacing (nm)	FWHM (°)	Crystal size (nm)	Thickness (nm)
XG-C	0.3354	1.67	5.2	2
XG-H	0.3343	0.38	31.1	11 - 15
XG-M	0.3339	0.40	28.8	6
GS	0.3342	0.65	15.2	12
GNP-COOH	0.3339	0.47	23.1	< 50
GNP-O_2	0.3335	0.36	33.6	< 50

The laser light scattering (LLS) method was used to measure the lateral size distribution of the bulk GNPs. The particle size distribution follows a log-normal distribution as shown in Figure 2.

The mean values of the effective particle diameters are taken as the lateral dimensions of the platelets. These were measured to be 0.20 μm for the XG-C, 1.04 μm for the XG-H, 16.05 μm for the XG-M and 1.27 μm for the GS GNPs respectively.

The lateral dimensions and thickness of the GNPs were also measured visually using the FEGSEM. The samples were prepared by sonicating the GNPs in THF for 10 min, and then dried in air for 5 min. They did not require any coating as they are already conductive. The samples were placed directly onto a SEM stub using conductive tape. Loose particles were then removed using compressed air to prevent contamination of the sample cham-

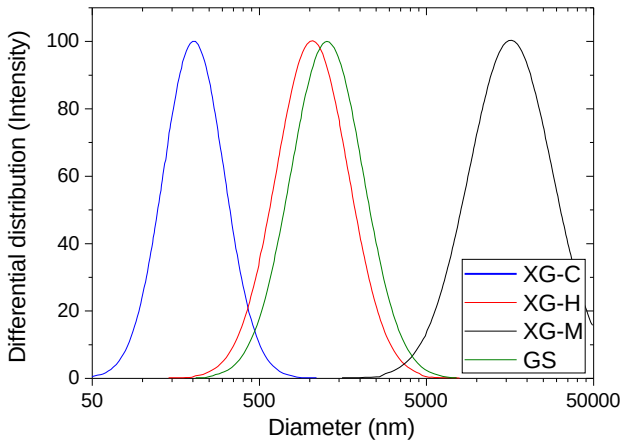

Figure 2: Particle diameter differential distribution measured by laser light scattering on linear-log scale.

ber. Selected images are shown in Figure 3. The XG-C GNPs, which have the smallest effective diameters as measured using LLS, resemble a relatively low aspect ratio particulate rather than a platelet structure, as shown in Figure 3(a). The XG-H, GS, GNP-COOH and GNP-O2 GNPs appeared to be similar in size, and the XG-M GNPs were clearly the largest. The graphite flake agglomerates, as shown in Figure 3(g), were approximately 15 μm in lateral size and 10 μm in thickness. The sheets of graphene were folded over each other, with very few individual platelets.

There were several features that were identifiable from the FEGSEM micrographs. Firstly, wrinkles were observed in the XG and GS GNPs, as shown in Figures 4(a) and 4(b). These GNPs were manufactured using an acid exfoliation method, which leaves trace amounts of hydroxyl and carbonyl functional groups. The local strains and electrostatic repulsion caused by the presence of these functional groups are thought to be the cause of the excessive wrinkling [32]. In contrast, the plasma process used to manufacture

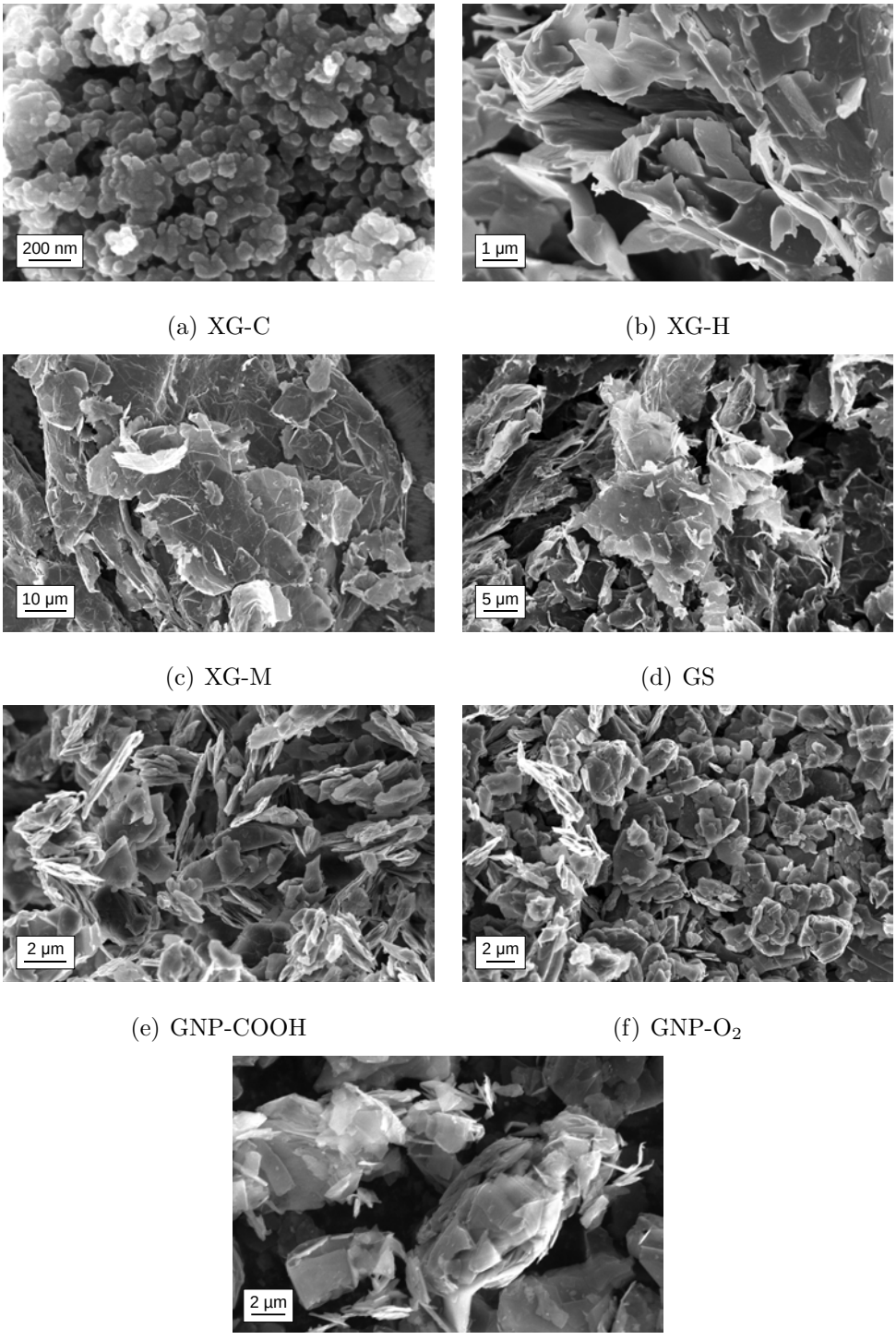

(a) XG-C

(b) XG-H

(c) XG-M

(d) GS

(e) GNP-COOH

(f) GNP-O_2

(g) Graphite flakes

Figure 3: FEGSEM micrographs of GNPs and GFs after 20 mins of ultrasonication in THF and drying in air.

the Haydale GNPs appears to cause less wrinkling, as shown in Figures 3(e) and 3(f), even though similar functional groups are present.

The edges of the GNPs were also observed to be damaged rather than having perfectly straight interfaces, as shown in Figure 4(c). Many of the platelets are folded and remain as multilayer platelets after ultrasonication, as shown in Figure 4(d).

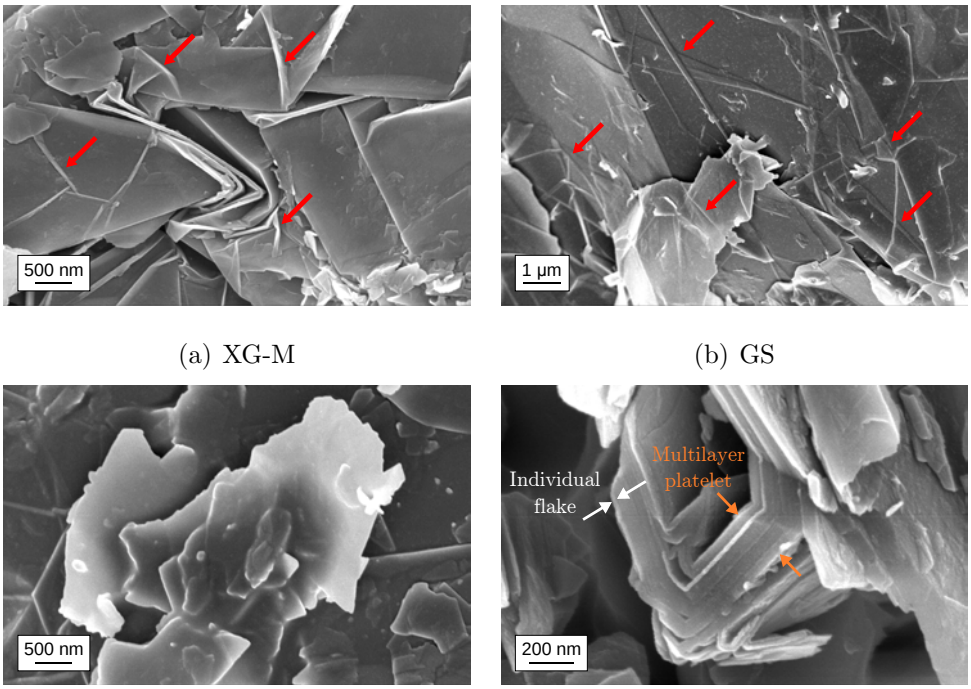

(a) XG-M (b) GS

(c) XG-H (d) GNP-O_2

Figure 4: FEGSEM micrographs of GNPs showing defects. Wrinkles on the GNPs are identified by the red arrows.

The lateral dimensions and thickness of the GNP flakes as measured are summarised in Table 3. The values of thickness quoted refer to the individual observable flakes, as shown in Figure 4(d). It was not expected that the platelets would be exfoliated because they will reagglomerate during the drying process. The individual graphene sheets are not distinguishable within the stack due to the limitations of the FEGSEM, where the resolution limit is 1.5 nm, whereas the individual graphene sheets are approximately 0.335 nm thick. The average thickness of the platelets was measured to be approximately 20 to 30 nm, which corresponds to 90 monolayers and agrees well with the XRD results. The stacking of the GNPs also appear to be highly ordered, corroborating the FWHM values from the XRD analysis.

Table 3: Modifier size measurements from laser light scattering and field emission gun scanning electron microscopy.

Modifier	Mean lateral size (μm)		Mean thickness	Aspect
	LLS	FEGSEM	(nm)	ratio
XG-C	0.20	0.3 ± 0.1	16 ± 4^a	19
XG-H	1.04	3.2 ± 1.7	31 ± 7	103
XG-M	16.1	21.7 ± 9.4	19 ± 9	1142
GS	1.27	3.9 ± 1.6	19 ± 6	205
GNP-COOH	–	2.3 ± 1.0	27 ± 9	85
GNP-O_2	–	2.4 ± 0.8	29 ± 9	83
GF	–	–	25 ± 12	–

[a] Defined as particulate diameter as the XG-C GNP was not observed as a platelet structure.

The mean lateral sizes measured from the FEGSEM micrographs were

generally larger than the effective particle diameters measured from LLS. The results from the two techniques are not expected to be equal as the laser light scattering technique gives an intensity-weighted differential size distribution, whereas the microscopy technique gives a number-weighted distribution. However, the trend between the two techniques shows good agreement; the XG-C GNPs have the smallest lateral size, the XG-M GNPs have the largest lateral size and the XG-H and GS GNPs were approximately equal in size. The XG-C GNPs did not have a platelet-like structure and thus the mean lateral size was approximated to be the size of each particulate agglomerate. This also increases the value of FWHM from the XRD results, as shown in Table 2.

3.2. XPS Spectra

Figure 5 shows the XPS survey spectra of the bulk GNP powders. For all of the GNPs, the C1s (∼284 eV) and O1s (∼531 eV) signals are clearly defined. Additionally, weak signals that are characteristic of N1s (∼399 eV), Si2p (∼103 eV) and S2p (∼168 eV) were detected. The high resolution, core level C1s spectra, reveal that there was only one peak at 284.2 eV, corresponding to the C-C bond [33]. This was unsurprising given that the GNPs are composed primarily of carbon with atomic concentrations above 90%, as shown in Table 4.

The atomic concentrations of each element present on the surface of the GNPs are summarised in Table 4. The carbon content of the GNPs from XG Sciences (XG-H, XG-M and XG-C) and Graphene Supermarket (GS) were measured to be lower than the manufacturer's quoted values [18–21]. Trace elements of nitrogen, fluorine, silicon and sulphur were detected and were

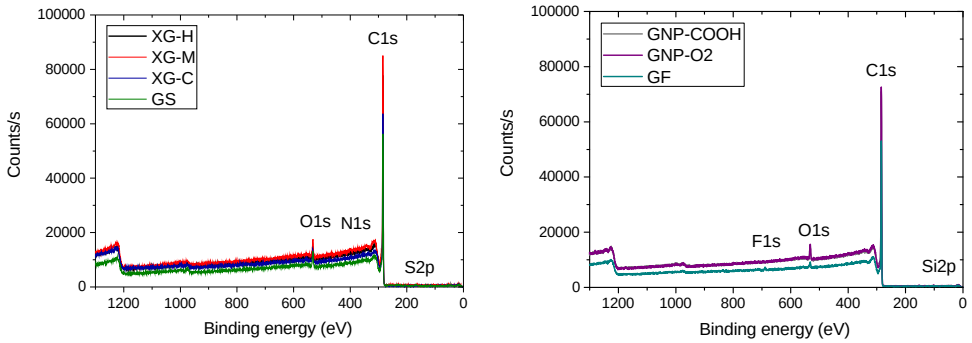

Figure 5: XPS survey spectra of bulk GNPs.

typically less than 1 at.%. The XG-M and GS GNPs had comparatively low carbon contents and high oxygen content. This can be indicative of the relatively poor quality of the GS GNPs, as elements other than carbon are present as functional groups at defect sites and edges. Indeed, a higher FWHM value was measured from the XRD for the GS GNP, indicating higher disorder in the crystal structure. The XG-H GNPs have the highest carbon content (96.1 at.%), which is of similar magnitude to the graphite flakes (GF).

The functionalised GNPs from Haydale (GNP-COOH and GNP-O_2) contain approximately 6 at.% of oxygen, which agrees well with the manufacturer's data sheet. It is of note that this value of oxygen content is not significantly higher than for the GNPs that were not functionalised (XG and GS GNPs). This is because the functional groups were only attached to the edges, dislocation sites and defects, similar to the other GNPs. However, there is insufficient information regarding what functionalities these oxygen elements are present as. This has a significant impact on the platelet/matrix adhesion, as even though the GS GNP has the highest oxygen content, it is

Table 4: Atomic percentage of GNP surface element composition.

Modifier	Element (at.%)					
	Carbon	Oxygen	Nitrogen	Fluorine	Silicon	Sulphur
XG-C	94.10	5.18	0.71	–	–	–
XG-H	96.08	3.92	–	–	–	–
XG-M	92.43	5.87	0.99	–	–	0.70
GS	91.58	7.53	–	–	–	0.89
GNP-COOH	94.07	5.61	–	–	0.31	–
GNP-O_2	93.17	6.51	–	–	0.33	–
GF	95.89	3.21	–	0.90	–	–

still poorly bonded to the epoxy matrix. By comparison, the GNP-COOH and GNP-O_2 GNPs have slightly lower oxygen contents but were found to be well bonded to the epoxy matrix (compare Figure 19(c) to Figure 21).

3.3. Morphology

The dispersion of the graphene nanoplatelets was examined from the FEGSEM images of the fracture surfaces of the GNP modified epoxy polymers. This does not give the true dispersion of the GNPs because of the many step changes as the crack propagates, visible as river lines, and the pullout of the GNPs, which can appear as voids, but can give an indication of the quality of dispersion.

The GNPs dispersed in THF first were found to be heavily agglomerated, as shown in Figure 6 for the 1.0 wt% XG-H-THF modified epoxy. The large agglomerates, typically of 50–100 μm, are highlighted in red and there were

also some smaller platelets dispersed, indicated by the red arrows. The extent of agglomeration can be observed at higher magnification, as shown in Figure 6(b), where significant clustering of the platelets can be seen.

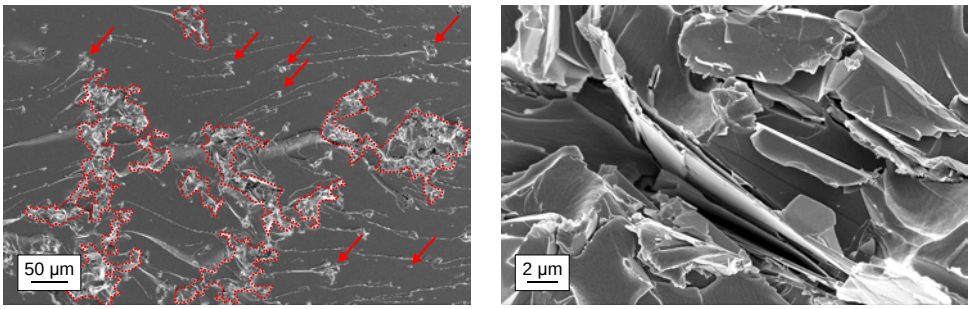

(a) x500 magnification (b) x10k magnification

Figure 6: FEGSEM micrograph of 1.0 wt% XG-H-THF modified epoxy. Regions enclosed in red are large agglomerates and the smaller agglomerates of GNP indicated by red arrows.

The GNPs that were sonicated in NMP were more evenly dispersed, as shown in Figure 7 for the 1.0 wt% XG-H-NMP modified epoxy. For both solvents, the GNPs were dispersed as stacked platelets, rather than as individual platelets. For both dispersions in THF and NMP, no polymer was found between the layers, hence the structure can be described as particulate rather than intercalated or exfoliated [34].

The XG-M, XG-C and GS GNPs show similar trends in dispersion when comparing the two solvents, as shown in Figure 8. The XG-M GNPs have a much larger lateral size and this can result in a more agglomerated structure than the other GNPs. The sizes of the agglomerates were measured for each of the GNP modified epoxies from the fracture surfaces, and the agglomerates of XG-M GNPs were up to 300 μm and 30 μm in length when dispersed in THF and NMP, respectively. This is compared to 150 μm and 100 μm for the

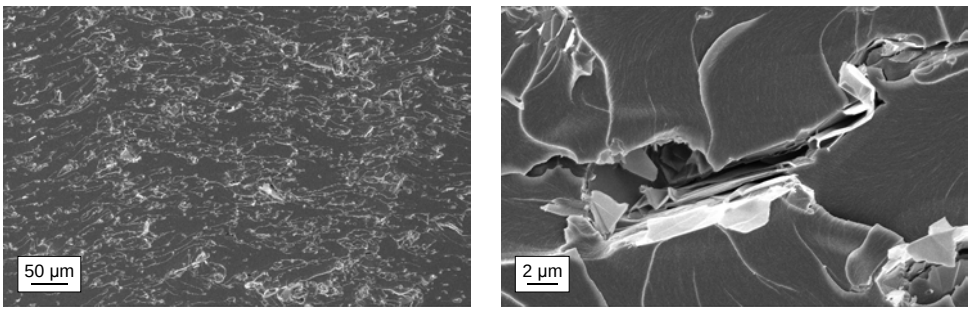

(a) x500 magnification (b) x10k magnification

Figure 7: FEGSEM micrograph of 1.0 wt% XG-H-NMP modified epoxy.

XG-H and GS GNPs dispersed in THF, respectively. Both the XG-H and GS GNPs dispersed in NMP have agglomerates of approximately 20 μm in size. The consequence of agglomeration is a lower effective aspect ratio and this can have a negative effect on the mechanical and fracture properties. The agglomerates of XG-C-THF GNPs were up to 4 μm in length. Particulates as small as 100 nm were observed for the XG-C-NMP GNP modified epoxy polymers.

At a GNP concentration of 1.0 wt%, the COOH and O_2 functionalised GNPs were found to be well dispersed as stacks of platelets approximately 60 μm in size, as shown in Figure 9. These are smaller than the agglomerates found for the GNPs that had not been functionalised and sonicated in THF. The individual stacks of platelets had smooth surfaces but appear to be damaged at the edges, as shown in Figure 10.

On examination of the GNP-COOH and GNP-O_2 GNPs at higher magnifications, such as those in Figure 10, the stacks of GNPs within the agglomerates appear to be broken into sub-micron lateral sized platelets, presumably by the sonication process. Zaldivar *et al.* [35] found that O_2 plasma

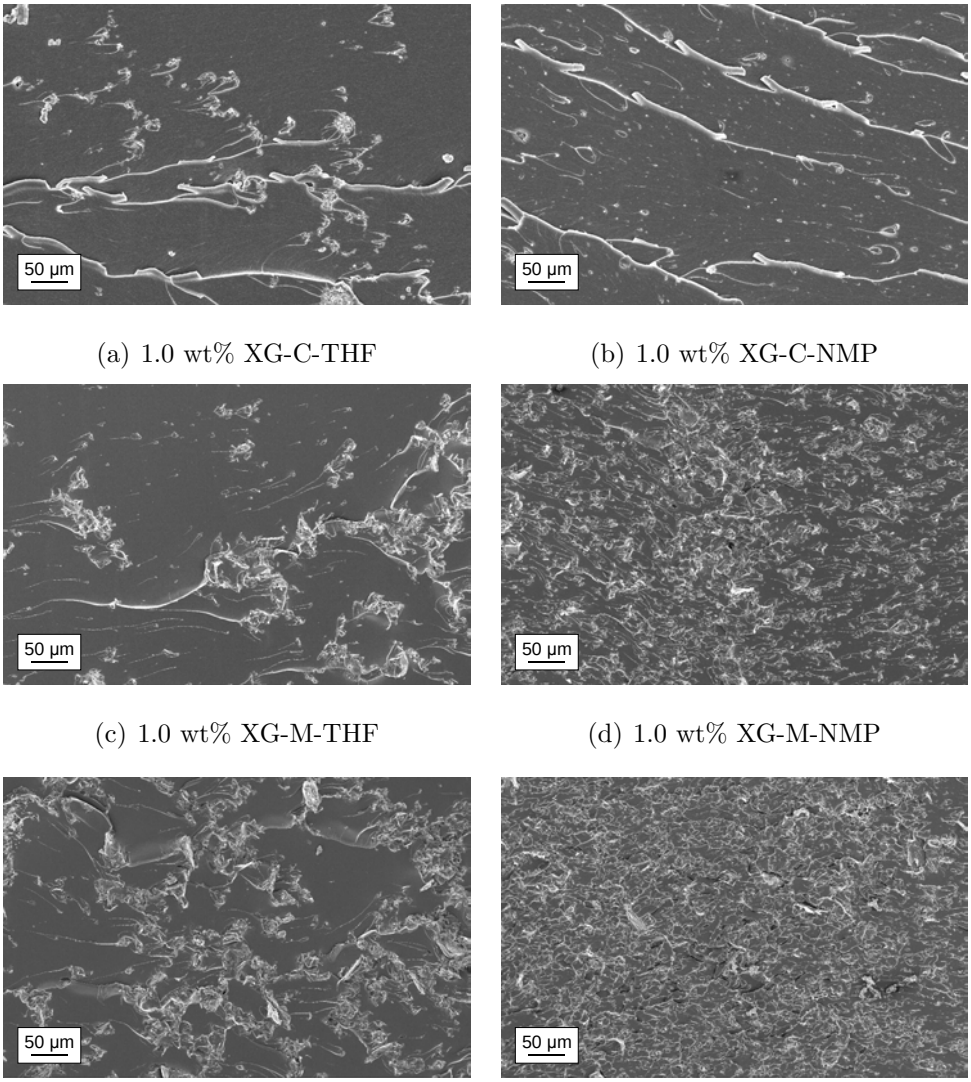

(a) 1.0 wt% XG-C-THF (b) 1.0 wt% XG-C-NMP

(c) 1.0 wt% XG-M-THF (d) 1.0 wt% XG-M-NMP

(e) 1.0 wt% GS-THF (f) 1.0 wt% GS-NMP

Figure 8: FEGSEM micrograph of GNP modified epoxy.

treatment can also damage the GNPs, seen as voids throughout the platelet surface and edges.

The graphite flakes were heavily agglomerated, as shown in Figure 11,

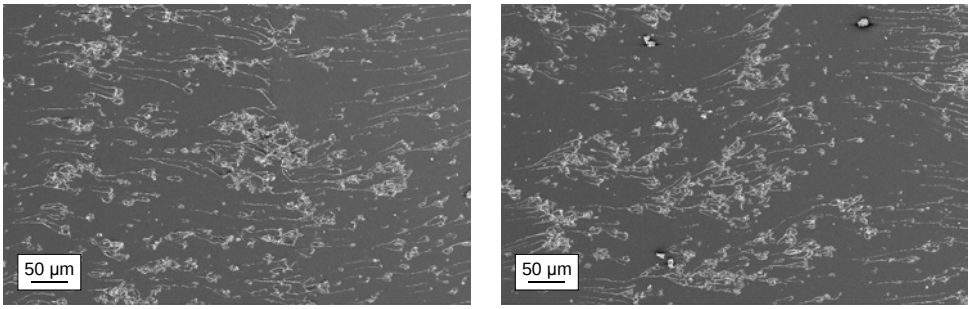

(a) GNP-COOH (b) GNP-O_2

Figure 9: FEGSEM micrograph of epoxy modified with 1.0 wt% functionalised GNPs.

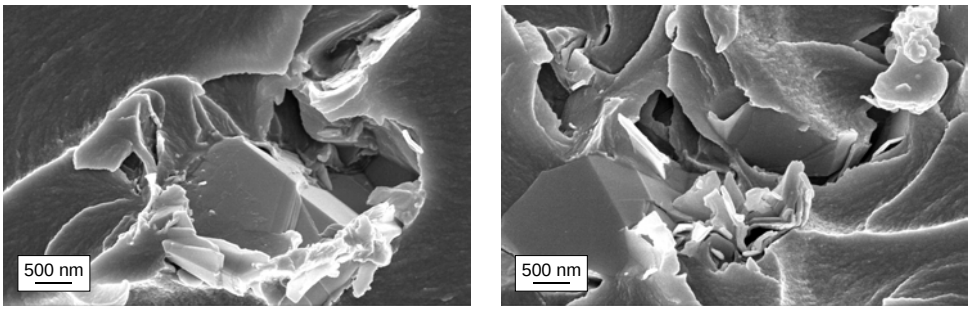

(a) GNP-COOH (b) GNP-O_2

Figure 10: FEGSEM micrograph of epoxy modified with 1.0 wt% functionalised GNPs at higher magnification.

where the large agglomerates are highlighted in red. Each graphite flake was observed to comprise up to 50 stacked plates, which were poorly adhered to the epoxy matrix as indicated by the smooth surfaces of the debonded platelets in Figure 11(b).

3.4. Thermomechanical properties

The glass transition temperature, T_g, of the epoxy was measured for the unmodified epoxy, epoxy with solvents (evaporated and unevaporated) and GNP modified epoxy. The T_g of the unmodified epoxy was measured to be

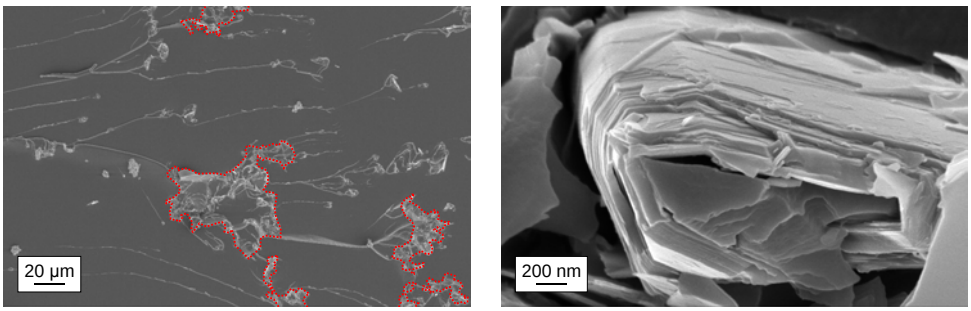

(a) x1000 magnification (b) x100k magnification

Figure 11: FEGSEM micrograph of graphite flake modified epoxy. Regions enclosed in red are large agglomerates.

157 °C. The tetrahydrofuran (THF) had little effect on the T_g when it was evaporated, but the n-methyl-pyrrolidone (NMP) reduced the T_g by 10 °C, as shown in Table 5. This indicates that NMP may have reacted with the epoxy resin prior to solvent removal. Both solvents reduced the T_g significantly if they were not removed, and this is an indication of the decrease in crosslink density of the epoxy.

The glass transition temperatures of the 1.0 wt% GNP modified epoxy polymers are summarised in Table 6. The addition of the GNPs from XG Sciences reduced the T_g of the epoxy with increasing GNP content, irrespective of the size of the nanoplatelets. In general, the GNPs dispersed in NMP exhibited lower glass transition temperatures than the GNPs dispersed in THF, similar to the trend observed for the unmodified epoxies. The GS modified epoxies in particular show significant reductions in the T_g with GNP content compared to the unmodified epoxy. This is caused by the entrapment of solvent, rather than an interaction between the GNPs and the epoxy, as the GNPs that were dispersed without solvent into the same epoxy did not affect

the T_g significantly.

The decrease in T_g associated with the higher loadings of GNP is caused by the increase in solvent required to disperse the GNPs. The GNP powder has a very low density, and thus requires a relatively large volume of solvent to disperse satisfactorily. This increase in the amount of solvent results in a longer time required to remove the solvent, which at elevated temperatures can cause a reaction between the solvent and the epoxy resin. The GNP-COOH and GNP-O_2 modified epoxies show a small decrease in T_g with modifier content as the carboxyl and carbonyl functional groups can react with the epoxy resin [36]. The graphite flakes, GF, have a high purity and did not affect the T_g of the epoxy.

Table 5: Glass transition temperature, Young's modulus, tensile yield stress, fracture toughness and fracture energy for anhydride cured DGEBA with solvents. The 'e' refers to solvent which was evaporated before curing the epoxy.

	T_g (°C)	E_t (GPa)	σ_y (MPa)	K_c (MPa m$^{1/2}$)	G_c (J/m^2)
Unmodified	157	2.9 ± 0.1	86 ± 0	0.64 ± 0.03	96 ± 9
10% THFe	155	3.0 ± 0.1	67 ± 2	0.58 ± 0.03	72 ± 7
10% THF	107	3.0 ± 0.0	71 ± 0	0.81 ± 0.05	103 ± 7
10% NMPe	147	3.0 ± 0.0	80 ± 3	0.51 ± 0.01	72 ± 5
10% NMP	87	2.9 ± 0.1	60 ± 2	0.73 ± 0.03	112 ± 9

3.5. Mechanical properties

The Young's modulus, E_t, of the unmodified epoxy was measured to be 2.9 GPa, see Table 6. The use of solvents did not affect the E_t of the epoxy,

Table 6: Glass transition temperature, Young's modulus, tensile yield stress, fracture toughness and fracture energy for the 1.0 wt% GNP modified epoxies.

	T_{g} (°C)	E_t (GPa)	σ_y (MPa)	K_{C} (MPa m$^{1/2}$)	G_{C} (J/m^2)
Unmodified	157	2.9 ± 0.1	86 ± 0	0.6 ± 0.0	96 ± 9
XG-C-THF	150	3.0 ± 0.0	67 ± 6	0.62 ± 0.05	84 ± 9
XG-C-NMP	152	3.2 ± 0.1	73 ± 5	0.59 ± 0.05	82 ± 11
XG-H-THF	151	3.1 ± 0.0	54 ± 2	0.85 ± 0.02	191 ± 10
XG-H-NMP	146	3.4 ± 0.1	64 ± 8	0.82 ± 0.01	144 ± 20
XG-M-THF	153	3.3 ± 0.1	50 ± 2	0.82 ± 0.05	145 ± 11
XG-M-NMP	150	3.3 ± 0.1	69 ± 2	0.88 ± 0.03	162 ± 4
GS-THF	138	3.1 ± 0.0	52 ± 4	0.88 ± 0.03	222 ± 20
GS-NMP	133	3.6 ± 0.1	50 ± 8	0.95 ± 0.04	212 ± 17
GNP-COOH	151	3.0 ± 0.2	72 ± 8	0.69 ± 0.05	134 ± 6
GNP-O_2	155	3.0 ± 0.0	65 ± 9	0.61 ± 0.04	99 ± 6
GF	159	3.1 ± 0.1	78 ± 4	0.68 ± 0.04	133 ± 12

as shown in Table 5, however did reduce the tensile strength, σ_t, and tensile strain at break, ε_B, even when the solvents were removed prior to curing, as shown in Figure 12(a). The yield strength of the epoxy was also reduced significantly when the solvent was not removed as the solvent plasticises the epoxy; note how the stress-strain curves for the case when the solvents were evaporated follow that of the unmodified epoxy exactly.

Typical true stress-strain curves for the unmodified and 2.0 wt% XG-H

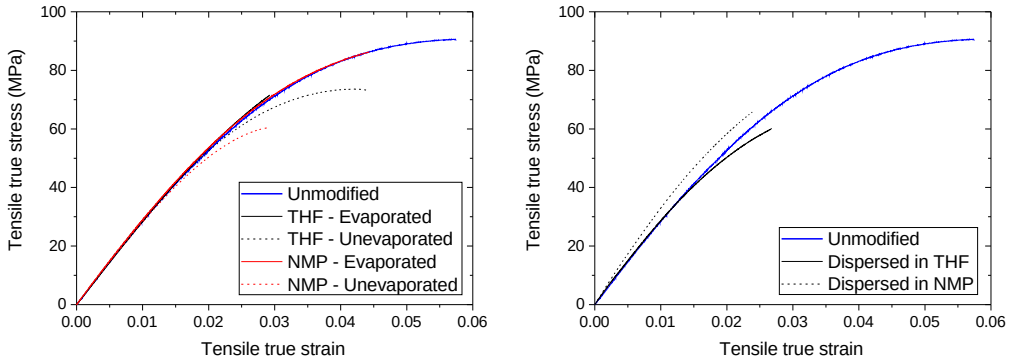

(a) 10 wt% solvent (b) 2.0 wt% XG-H

Figure 12: Typical tensile true stress-strain curves.

GNP modified epoxy, with the GNPs dispersed in THF and NMP, are shown in Figure 12(b). For both solvents, the addition of 2.0 wt% XG-H GNP to the epoxy reduced the ε_B significantly from 5.7% to 2.3% due to the GNP agglomerates.

The E_t of the epoxy increases with GNP content as summarised in Table 6. This was expected given the high modulus of the GNPs [37]. The epoxies modified with GNPs dispersed in THF typically had a lower value of E_t than the GNPs dispersed in NMP. The E_t of the 1.0 wt% XG-H modified epoxy when dispersed using THF was measured to be 3.1 GPa, whereas the GNPs dispersed using NMP was measured to be 3.6 GPa. This is because of the agglomeration of the platelets when dispersed in THF. The effect of agglomeration is to reduce the effective aspect ratio of the GNPs, which in turn reduces the stress transfer to the GNPs, and hence reduces the stiffening effect.

The plane strain compressive true stress-true strain curves for the unmodified and 10 wt% solvent modified epoxies, both dissolved and evaporated,

are shown in Figure 14. The trends observed in the plane strain compression tests were similar to the tensile tests. The compressive properties were unaffected when the solvents were removed prior to curing, whereas the yield strength was reduced by up to 26% when the solvents remained in solution in the epoxy due to plasticisation. This effect can be used to determine whether solvent remains dissolved in the epoxy in the GNP modified epoxies. It would not be possible to identify this from the tensile tests as the brittle materials fracture before yielding occurs. The compressive true yield stress, σ_{yc}, of the epoxies with unevaporated solvents was lower for the NMP modified epoxy than the THF modified epoxy due to the different molecular mass of the two solvents.

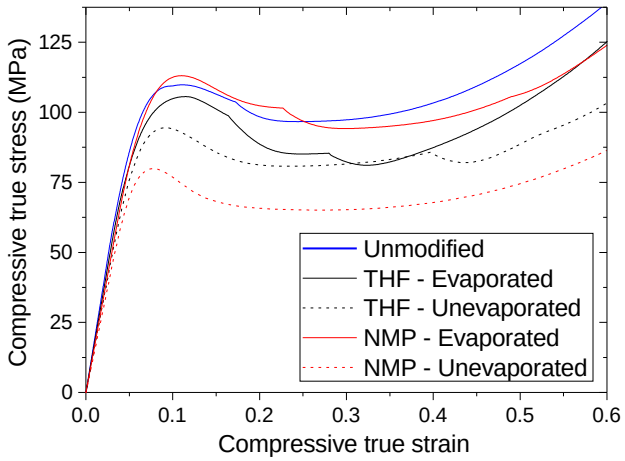

Figure 13: Compressive true stress-true strain curves for unmodified and 1 wt% GS GNP and GF modified epoxy polymers.

With the addition of 1.0 wt% of GNPs, there were little or no differences in the elastic region during plane strain compression, as shown in Figure 14. The value of σ_{yc} remains constant, which indicates that most of the solvent

has been removed prior to curing. Furthermore, the presence of the GNPs appears to have caused the samples to fracture earlier. Finally, samples from the centre of the compressed regions were sectioned and placed between cross polarisers in an optical microscope, and there was no evidence of localised shear yielding observed.

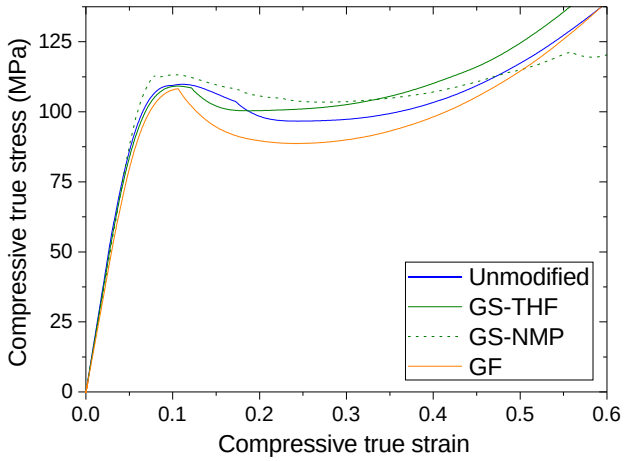

Figure 14: Compressive true stress-true strain curves for unmodified and 10 wt% solvent modified epoxy polymers.

3.6. Fracture performance

The values of K_C and G_C for the unmodified epoxy were measured to be 0.64 MPa $m^{1/2}$ and 96 J/m^2, respectively. The fracture performance was unaffected when the solvents were added to the epoxy resin and subsequently evaporated. However, the fracture energy decreased to 72 J/m^2 when the solvents were not removed, as shown in Table 5, due to the plasticisation of the epoxy.

Interestingly, the G_C and K_C values of the epoxy modified with GNPs dispersed in THF and with GNPs dispersed in NMP were roughly equivalent

within experimental error, as shown in Figure 15. This suggests that the agglomeration of the GNPs at the micron scale does not affect the fracture performance of the GNP nanocomposites.

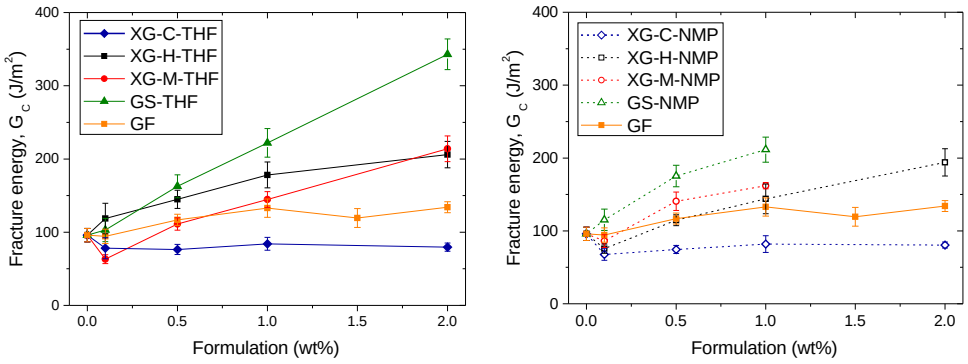

(a) Dispersed in THF

(b) Dispersed in NMP

Figure 15: Fracture energy, G_C, for the various GNP modified epoxy polymers.

The addition of the GNPs at low loadings, such as that at 0.1 wt%, did not affect significantly the toughness of the epoxy polymer. At higher concentrations, the addition of the intermediate sized GNPs (XG-H, XG-M and GS) led to an increase in the G_C of the epoxy. A maximum G_C of 343 J/m^2 was measured for the 2.0 wt% GS-THF modified epoxy, corresponding to an increase of 240%. The XG-M GNPs, which have the largest lateral dimension and aspect ratio, were heavily agglomerated and showed poor fracture performance at a maximum G_C value of 214 J/m^2 for the 2.0 wt% XG-M-THF modified epoxy.

The XG-C GNPs and GF modified epoxies did not have any affect on the G_C of the epoxy polymer. The G_C of the XG-C GNP and GF modified epoxies remained constant at about 80 J/m^2 and 134 J/m^2, respectively, up to 2.0 wt%. The functionalised GNPs (GNP-COOH and GNP-O_2) also did

not have a significant effect on the fracture performance of the epoxy, as shown in Figure 16. These will be discussed in the following section.

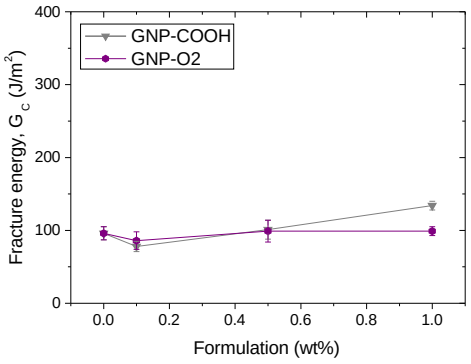

Figure 16: Fracture energy, G_C, for the functionalised GNP modified epoxy polymers.

3.7. Toughening mechanisms

The fracture surfaces were observed using scanning electron microscopy and the direction of crack propagation is from right to left. The fracture surfaces of the unmodified epoxy appear smooth, and feature only riverlines that represent step changes in height as the crack propagates. Crack forking and the multi-planar nature of the surface observed here are the main mechanisms to absorb excess energy in such brittle materials [38].

With the addition of the GNPs, a much rougher appearance at the process zone indicates significant plastic deformation of the epoxy matrix was observed around the clusters of GNP. For the XG-H, XG-M and GS GNPs dispersed in THF evidence of crack deflection was observed, as shown in Figure 17. Crack deflection is seen as the crack paths being redirected around clusters of GNPs. Figure 17(b) shows the tails behind the GNPs which indicate crack deflection. The degree of toughening has a strong proportionality

to the aspect ratio of disc-shaped particles [39], i.e. platelets, and this was reflected in the G_C values.

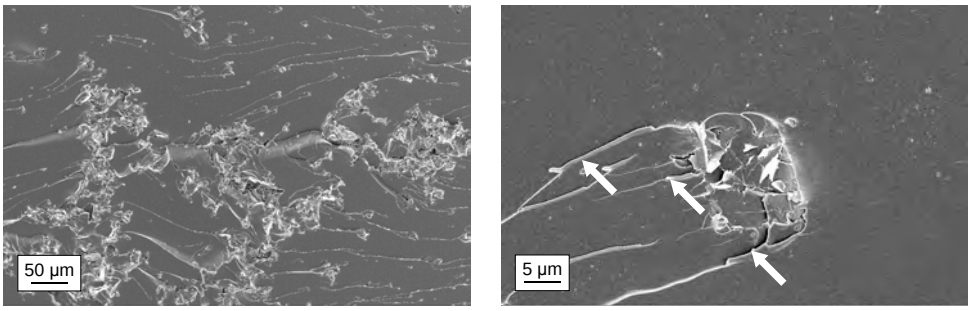

(a) x500 magnification (b) x5k magnification

Figure 17: FEGSEM micrograph of 1.0 wt% XG-H, dispersed in THF, modified epoxy fracture surfaces. Evidence of crack deflection is identified by white arrows.

The larger XG-M GNPs dispersed in THF were found to be agglomerated into much larger clusters. Figure 18 shows higher resolution FEGSEM micrographs of the XG-H-THF and XG-M-THF GNP modified epoxies. The XG-H GNPs remain flat with very few defects, while the XG-M GNPs are highly wrinkled and folded, as identified by the red arrows in Figure 18(b). This reduces the effective aspect ratio and hence has a negative effect on the mechanical properties of the XG-M modified epoxies.

For the XG-H, XG-M and GS GNPs dispersed in NMP, the main toughening mechanisms observed for the well dispersed GNPs were found to be debonding of the GNPs, followed by plastic void growth of the epoxy matrix, as shown in Figure 19. The large voids between the platelets could be caused by a void growth mechanism or by platelets which have been pulled out. While it would not be possible to identify the same GNPs on the other side of the fracture surface, the remaining platelets appear to have been pulled

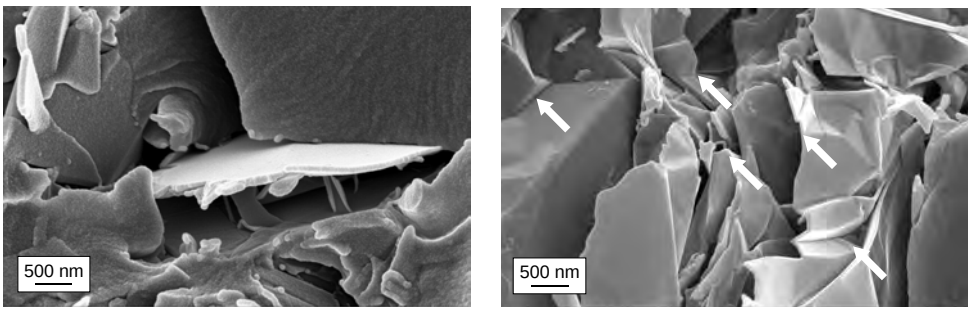

(a) XG-H (b) XG-M

Figure 18: FEGSEM micrograph of 1.0 wt% GNP, dispersed in THF, modified epoxy fracture surfaces. Defects on the XG-M GNPs are identified by the white arrows.

out. This effect was not seen away from the process zone, i.e. in the fast fracture zone.

The fracture surfaces of the XG-C GNPs dispersed in THF and NMP, as shown in Figure 20, show very little debonding and the degree of crack deflection is low due to the small size of the particulates. The better apparent adhesion of the GNPs to the epoxy is due to the small size, which results in more edges and hence functional groups (as these are at the edges). However, this does not result in an improvement in tensile properties due to the structure and quality of the GNPs, where the surfaces of the platelets appear rough and damaged.

The GNP-COOH and GNP-O_2 functionalised GNPs were well bonded to the epoxy, as shown in Figure 21, owing to the presence of the functional groups. This results in limited debonding, and hence little subsequent void growth. On-plane crack front interactions were also restricted by the relatively small size of the agglomerates of GNPs. Hence there is little toughening effect.

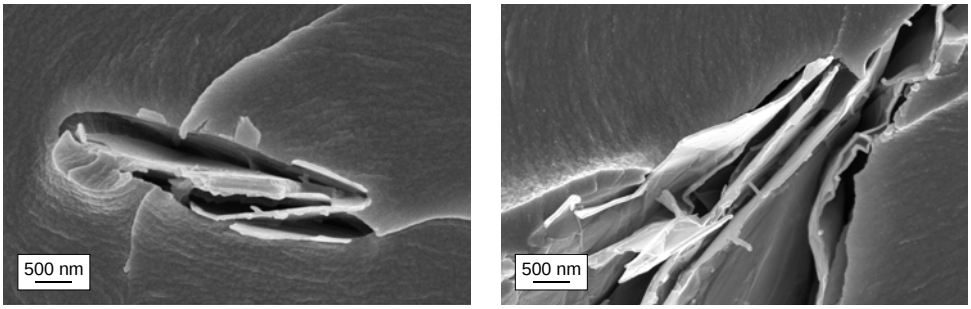

(a) XG-H (b) XG-M

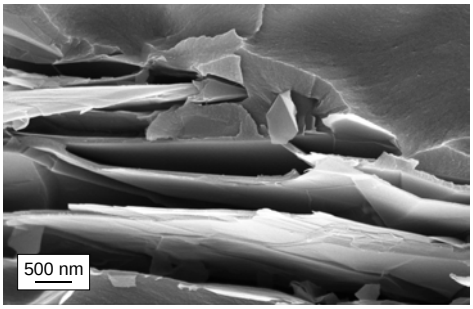

(c) GS

Figure 19: FEGSEM micrograph of 1.0 wt% GNP, dispersed in NMP, modified epoxy fracture surfaces.

The fracture surfaces of the graphite flake modified epoxy show limited plastic deformation of the epoxy matrix, see Figure 22(a), and crack tip interactions, see Figure 22(b). All of the graphite flakes were observed to have debonded, confirming the expected very poor adhesion between the flakes and the epoxy. Furthermore, there was little plastic deformation observed around the debonded graphite flakes, and hence little toughening effect.

None of the GNP modified epoxies showed any evidence of shear band yielding when thin sections from the compression samples were examined between cross polarisers. This contributes to the low level of toughening

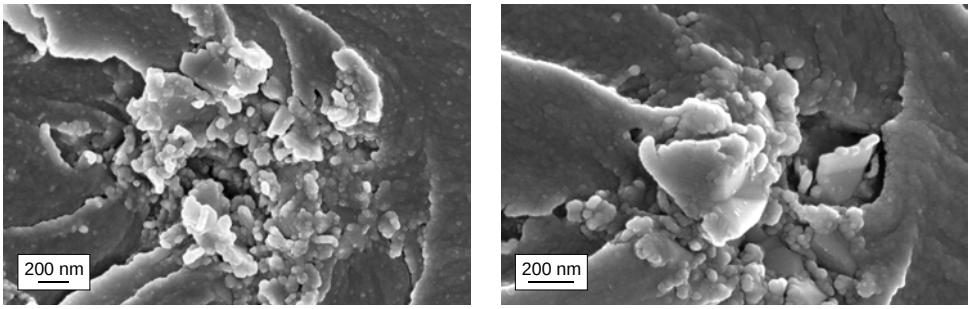

(a) Dispersed in THF (b) Dispersed in NMP

Figure 20: FEGSEM micrograph of 1.0 wt% XG-C GNP modified epoxy fracture surfaces.

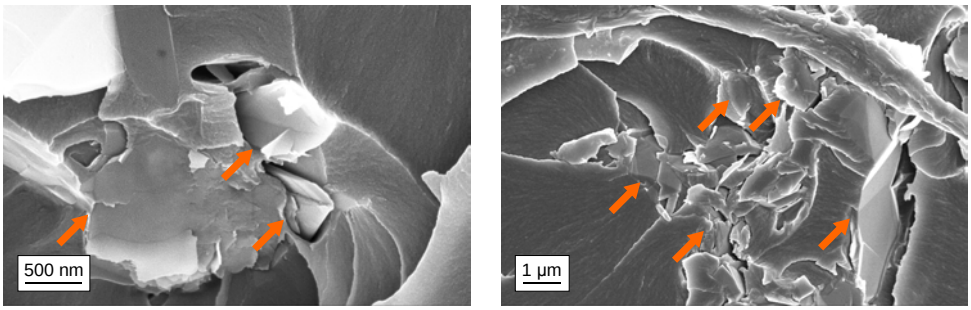

(a) GNP-COOH (b) GNP-O_2

Figure 21: FEGSEM micrograph of 1.0 wt% functionalised GNP modified epoxy fracture surfaces. Orange arrows indicate limited debonding and void growth.

observed from these modified epoxies as shear band yielding is generally accepted to be a major toughening mechanism [40].

To summarise the toughening mechanisms, the GNPs dispersed in THF exhibit crack deflection only and the GNPs dispersed in NMP show evidence of platelet debonding, pull-out and plastic void growth of the epoxy matrix.

3.8. Discussion

Within the field of graphene filled composites, there are several methods to produce these materials, each with its own advantages and disadvantages.

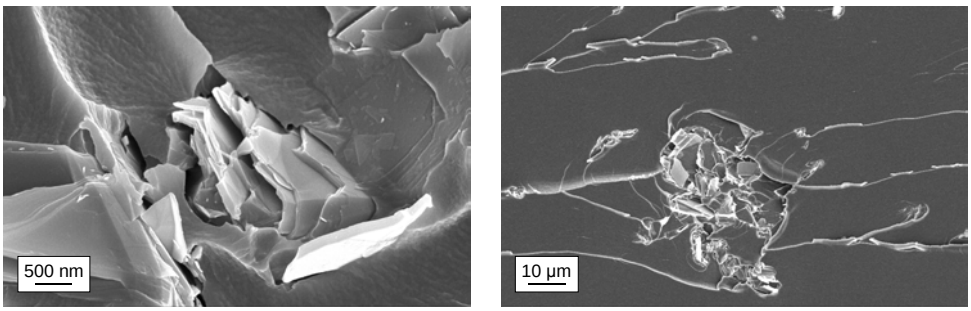

(a) (b)

Figure 22: FEGSEM micrograph of 1.0 wt% GF modified epoxy fracture surfaces.

As such, there is a large variation in results in the literature regarding the mechanical performance of graphene modified polymers. In this work, the factors that may contribute to this discrepancy in mechanical and fracture properties were examined, namely platelet size, aspect ratio, platelet quality, dispersion and surface functionalities.

Each of these factors were found to be important in contributing to the mechanical and fracture performance. In general, the larger platelet size, and hence aspect ratio, GNPs give higher values of modulus and G_{C}. This is due to the improved stress transfer in higher aspect ratio platelets based on shear lag theory [41]. For example, at 2.0 wt%, the XG-C-NMP (lateral size = 0.3 μm) increased the E_t from 2.9 GPa to 3.3 GPa, whereas the XG-H-NMP (lateral size = 3.2 μm) increased the E_t to 3.6 GPa. However, the largest GNPs (XG-M) did not disperse well and large agglomerates were observed. Large, higher aspect ratio platelets would also tend to wrinkle more. These types of defects reduce the effective aspect ratio of the GNPs, and thus reduce the overall contribution to the mechanical and fracture performance. As such, an optimum GNP lateral size of 3 – 4 μm was determined (XG-H

and GS). Furthermore, a minimum platelet size was observed to be required for toughening. Similarly, Kinloch and Taylor [34] found that silicates with larger diameters and aspect ratios were most efficient for toughening epoxy polymers.

The choice of solvents was also found to significantly affect the size of agglomerates. The GNPs sonicated in NMP first were found to be better dispersed as smaller agglomerates, compared to those sonicated in THF. This is because the exfoliation of the initially agglomerated GNPs is more effective when the surface energies of the solvent and graphene are similar in value [42], i.e. low energy is required for exfoliation. Typical values of surface tension for NMP and THF are 41 mN/m and 26 mN/m, respectively, and solvents with surface tension around 40 – 50 mN/m are known to have good solvent-graphite interaction [42, 43]. Exfoliation of the platelets was not observed, as they remained in stacks. A higher degree of shearing during processing (e.g. using a three-roll mill) than the low-shear conditions used here may encourage exfoliation.

The use of solvents to disperse the GNPs in the epoxy was required based on initial trials. When the GNPs were added directly into the resin, followed by ultrasonication, the GNPs were found to sediment at the bottom of the vertical moulds during the curing process. Dispersing the GNPs in solvent alleviated these problems. These settling issues were not observed for the functionalised GNPs, thus solvents were not used to disperse these GNPs. There was also the additional benefit of reducing the temperature of the mixture during sonication due to the evaporation of the solvents. Probe sonication can generate very high local temperatures near the tip which can

cause degradation of the epoxy resin.

Interestingly, the fracture energy was of similar values for the GNPs which were well dispersed as stacks of platelets, and for the GNPs that were heavily agglomerated. This was determined to be coincidence that the different toughening mechanisms produce similar energy contributions. Shear band yielding is typically a major toughening mechanism in rubber toughened epoxies. However, shear yielding was noticeably absent, as observed from the plane strain compression tests. There are several reasons that may cause this. The lack of plastic deformation of the epoxy could be a direct result of the lack of strain energy build up due to such early debonding, thus slowing the growth of shear bands and voids [44, 45]. Alternatively, these high aspect ratio GNPs have sharp edges which effectively act as defects and leads to fracture at low loads, hence low fracture toughness. Indeed, a much lower failure strain and stress was observed in the uniaxial tensile tests.

Unlike the trend observed from the tensile tests, the compressive modulus, E_c, and compressive true yield strength, σ_{yc}, did not show any significant changes with GNP content. The higher stresses in a plane strain compression test, due to the additional constraint, cause the GNPs to fracture at low strains, thus limiting the compressive modulus and strength. Secondly, although graphene as a bulk material has a much higher strength than epoxy (130 GPa compared to 86 MPa) [37], at such low concentrations, it would have little to no effect on the composite strength. The GNPs appear to be randomly aligned, thus would not provide significant reinforcement in the direction of the load.

Compared to other rigid modifiers, the 2.0 wt% GS-THF modified epoxy

has the highest value of G_C at 343 J/m^2. However, this is still low compared to the rubber modified epoxies which can have G_C values above 1000 J/m^2 [40]. Clearly, the GNP modified epoxies are still relatively brittle, even at the highest concentrations possible. Strong platelet/matrix adhesion from the functionalised GNPs do not appear to alleviate the deficit in G_C, as toughening mechanisms such as debonding and pull-out are inhibited. Interestingly, the GS GNPs have the highest oxygen content, but did not have strong platelet/matrix adhesion. This would suggest that the location and type of functional groups are more important than the oxygen content. It could also simply be due to the higher stress required to debond the smaller platelets (XG-C, GNP-COOH, GNP-O2 GNPs).

A relatively high Young's modulus can be achieved, as shown by the 2.0 wt% XG-H-NMP modified epoxy (3.6 GPa compared to 2.9 GPa for the unmodified epoxy). This is at much lower concentrations than achievable using silica nanoparticles (3.9 GPa at 20 wt%), showing the advantage of having high aspect ratio high-stiffness particles. Current research on graphene materials focuses on creating large (millimetre scale), pristine monolayers at high production rates [46]. These materials can bring substantial improvements, provided that they can be well dispersed as high aspect ratio platelets, of which studies are also being conducted [47]. However, there will be a maximum platelet size above which there is no further benefit of increased size, as for short fibres.

The graphite flakes had a minimal effect on the mechanical properties of the epoxy. It appears then that maintaining the lateral size while decreasing the thickness to the nano-scale with these GNPs, such as the XG-H or GS

GNPs, to achieve higher aspect ratios can indeed result in more significant improvements in mechanical and fracture properties. However, it should be noted that not all of the nanoplatelets have similar performance gains. The XG-C GNPs, which have a platelet size of 0.3 μm, were more particulate-like than platelet and did not have any significant effects on the mechanical properties. Similarly, the GNP-COOH and GNP-O_2 GNPs have little effect on the mechanical performance of the epoxy up to 1.0 wt%.

4. Modelling studies

4.1. Young's modulus

The Young's modulus of the GNP/epoxy composites can be modelled using existing analytical models. The Halpin-Tsai model [48, 49] is a semi-empirical model that calculates the composite modulus, E_c, as a function of matrix, E_m, and particle, E_p, modulus, taking into account the aspect ratio through the use of a shape factor, ζ. The composite modulus, E_c, is calculated by:

$$E_c = \frac{1 + \zeta \eta V_f}{1 - \eta V_f} E_m \tag{4}$$

where ζ is the shape factor, V_f is the volume fraction of particles and η is given by:

$$\eta = \frac{\frac{E_p}{E_m} - 1}{\frac{E_p}{E_m} + \zeta} \tag{5}$$

van Es [50] suggested that for the calculation of axial (11) and transverse (33) moduli of composites with platelet type fillers, the following shape factors should be used:

$$\zeta_{11} = \frac{2w}{3t} \tag{6}$$

$$\zeta_{33} = 2 \tag{7}$$

The Mori-Tanaka model [51] predicts the elastic behaviour of a two-phase composite while taking into account particle interactions, assuming a homogeneous dispersion and perfectly bonded interface. Equations for the Mori-Tanaka model for platelets with an aspect ratio not equal to one were derived by Tandon and Weng [52]. The composite modulus when the platelets are aligned with the long axis parallel to the loading direction, E_{11}, is given by:

$$E_{11} = \frac{E_m}{1 + V_f \left(A_1 + 2v_m A_2\right) / A} \tag{8}$$

The transverse composite modulus, E_{33}, is given by:

$$E_{33} = \frac{E_m}{1 + V_f \left(-2v_m A_3 + \left(1 - V_f\right) A_4 + \left(1 - V_f\right) A_5 A\right) / 2A} \tag{9}$$

where V_f is the filler volume fraction, v_m is the Poisson's ratio of the matrix, and the variables A_1, A_2, A_3, A_4 and A_5 are functions of volume fraction, aspect ratio and Poisson's ratio of the matrix and fillers, and are given in [52]. Finally, the modulus of a composite with randomly oriented particles can be estimated using [50]:

$$E_c = 0.49E_{11} + 0.51E_{33} \tag{10}$$

A platelet modulus, E_p, of 1000 GPa [37] and a Poisson's ratio, ν_p, of 0.3 were used. The matrix modulus, E_m, and Poisson's ratio, ν_m, were measured experimentally. The volume fractions were calculated using the weight percentages and a graphene density of 2.2 g/cm^3. The platelet thickness and lateral sizes measured from the FEGSEM micrographs were used to calculate the aspect ratios, see Table 3. The composite modulus when the platelets

are aligned with the long axis parallel to the loading direction is referred to as "parallel", i.e. E_{11}, and the composite modulus with randomly oriented platelets is referred to as "random".

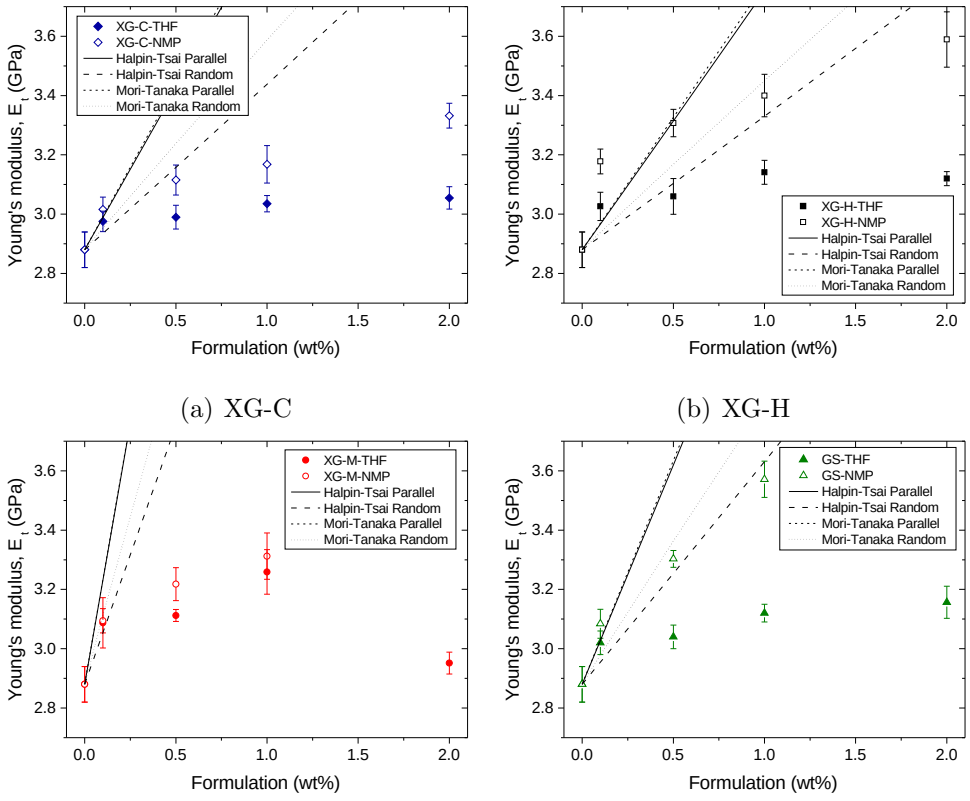

(a) XG-C (b) XG-H

(c) XG-M (d) GS

Figure 23: Analytical models for Young's moduli of GNP modified epoxy polymers.

The Halpin-Tsai "random" predictions show good agreement with the XG-H-NMP and GS-NMP modified epoxies. For the other GNP modified epoxies shown, the models can predict the composite moduli at low loadings such as at 0.1 wt%, however they begin to deviate from the experimental results as agglomeration reduces the effective aspect ratios of the modifiers

with increasing GNP content. As a consequence, the models significantly overpredict the Young's modulus at higher loadings. For both the Halpin-Tsai and Mori-Tanaka models, the aspect ratio is the factor that has the most significant effect on the composite modulus predicted. The models can be modified to take into account the reduction in aspect ratio [53], however the introduction of such constants tend to be strictly systematic and changes depending on the system used. The Halpin-Tsai and Mori-Tanaka "parallel" models were relatively close in value, however there were more deviations in the "random" arrangement as the concentration is increased.

4.2. Fracture energy

The major toughening mechanism observed for the GNPs dispersed in THF was crack deflection, whereas debonding, followed by platelet pull-out and plastic void growth were observed for the GNPs dispersed in NMP. The composite fracture energy can be estimated using the Huang and Kinloch [28] approach:

$$G_{IC} = G_{CU} + \psi \tag{11}$$

where G_{CU} is the fracture energy of the unmodified epoxy polymer and ψ represents the overall toughening contribution provided by the presence of the particulate phase:

$$\psi = \Delta G_{cd} + \Delta G_{db} + \Delta G_{po} + \Delta G_{v} \tag{12}$$

where ΔG_{cd} is the energy contribution from crack deflection, ΔG_{db} is the energy contribution from interfacial debonding, ΔG_{po} is the energy contribution from platelet pull-out, and ΔG_{v} is the energy contribution from void growth. Note that the optical microscopy of the PSC specimens showed that

no additional shear banding occurred from the addition of the GNPs, and so there is no contribution from this toughening mechanism.

The energy contribution from crack deflection, ΔG_{cd}, was derived by Faber and Evans [39] using a fracture mechanics approach. Green *et al.* [54] argued that for crack pinning the particles must be much larger than the plastic zone size. A similar argument can be made for crack deflection, where the particles should be larger than the crack opening displacement [55]. The GNP agglomerates were typically larger than 50 μm, and the crack opening displacements of these brittle materials are up to 10 μm; thus the Faber and Evans approach is applicable for this case. The integrals in the analytical model were solved numerically using MATLAB.

The platelet debonding and pull-out mechanisms were calculated using a similar approach to that of Hull and Clyne [56] to obtain:

$$\Delta G_{db} = \frac{V_f L_d G_i}{t} \tag{13}$$

where V_f is the volume fraction, L_d is the debonded length, G_i is the interfacial fracture energy between the filler and matrix and t is the platelet thickness. Barber *et al.* [57] measured the interfacial fracture energy between MWCNTs and a polymer matrix and found a strong dependence between G_i and CNT radius. The measured values of G_i ranged from 4 to 70 J/m^2, comparable to other fibre reinforced polymers. For the current study, a value of $G_i = 25$ J/m^2 was used [53]. For the platelet pull-out mechanism:

$$\Delta G_{po} = \frac{V_f L^3 \tau_i}{3Lt} \tag{14}$$

where τ_i is the interfacial shear strength and L is the platelet length. The determination of τ_i is difficult as there are inherent problems in isolating

and manipulating individual platelets at the nanoscale. Errors may also be introduced in analytical or numerical models to determine this value. This is due to the assumptions made of the structure of these platelets, as there is a size distribution and they are not monodisperse. Barber *et al.* [57] found a size dependency between τ_i and the radius of multi-walled carbon nanotubes (MWCNT), however this could be due to sliding between each layer of the MWCNT. They determined experimentally that the maximum value of τ_i for the interface between a MWCNT and a polymer matrix was approximately 100 MPa. It was determined that this would be applicable as this is of the same order of magnitude of the tensile strength of the epoxy matrix.

The energy contribution due to plastic void growth can be written as [40]:

$$\Delta G_v = \left(1 - \frac{\mu_m^2}{3}\right)(V_{fv} - V_f)\,\sigma_{yc} r_{pz} K_{vm}^2 \tag{15}$$

where μ_m is a material constant [29], V_{fv} is the volume fraction of voids, V_f is the particle volume fraction, σ_{yc} is the plane strain compressive true yield stress, r_{pz} is the Irwin plane strain plastic zone radius and K_{vm} is the maximum stress concentration for the von Mises stresses around the particle. To calculate the contribution from the void growth of the matrix around a debonded platelet, some assumptions were made about the shape and size of the final void. It was assumed that the platelets were square and that the void grows to a final lateral size of $(1 + \gamma_f)L$ and thickness of $(1 + \gamma_f)t$, where γ_f is the failure strain of the unmodified epoxy measured from the plane strain compression tests.

The parameters used in the modelling of the GNP modified epoxies are tabulated in Table 7.

The predicted and measured values of fracture energy using the crack

Table 7: Parameters used in modelling fracture energy of GNP modified epoxies.

Name	Variable	Units	Value
Platelet length	L	nm	Table 3
Platelet thickness	t	nm	Table 3
Aspect ratio	AR	–	Table 3
Void length	L_v	μm	$(1+\gamma_f)L$
Void thickness	t_v	nm	$(1+\gamma_f)t$
Plane strain compressive yield true stress	σ_{yc}	MPa	107
Uniaxial tensile yield true stress	σ_{yt}	MPa	89
Plane strain compressive fracture true strain	γ_f	–	0.91
Pressure-dependent yield stress parameter [29]	μ_m	–	0.2
Unmodified epoxy fracture energy	G_{CU}	J/m^2	96
Interfacial fracture energy [53]	G_i	J/m^2	25
Interfacial shear strength [57]	τ_i	MPa	47

deflection model for the GNPs dispersed in THF are summarised in Figure 24. The debonding and void growth mechanisms were not observed from the fracture surfaces, thus were not considered in the model for the epoxies modified with GNPs dispersed in THF. The aspect ratios used were determined from Table 3. These were 25 for the XG-C, 100 for the XG-H, 1000 for the XG-M and 200 for the GS GNPs. The model assumes that all of the platelets cause crack deflection.

The fracture energy predictions using the crack deflection model agree well with the experimental results for the XG-H-THF and GS-THF modified epoxies. However, the XG-M-THF modified epoxies show poor agreement with the model with an aspect ratio of 1000, instead they agree well with the prediction for an aspect ratio of 100 as in the case for XG-H-THF. This

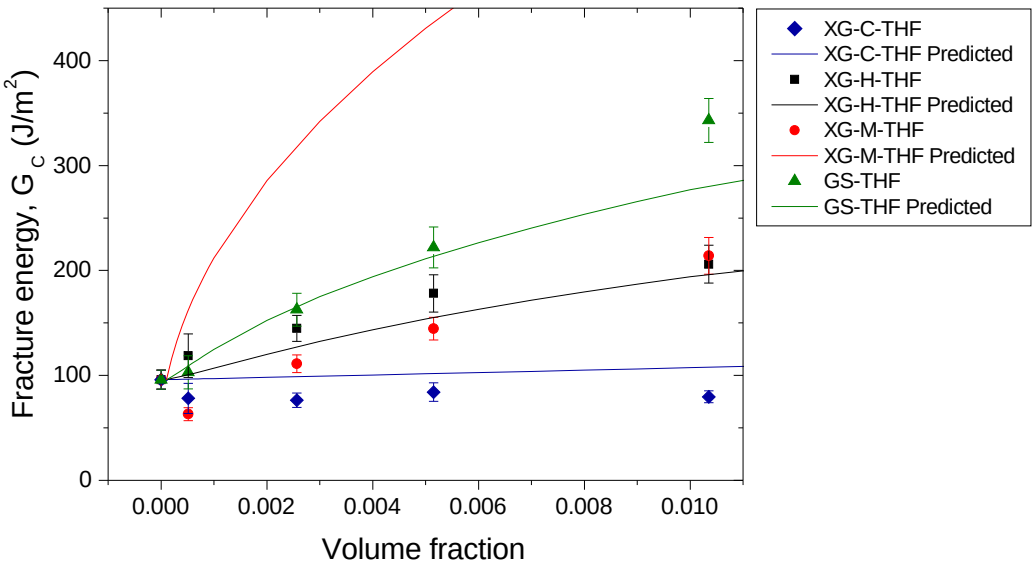

Figure 24: Predicted (crack deflection only) and measured values of fracture energy for epoxy polymers modified with GNPs dispersed in THF.

shows an indication of the degree of reduction in effective aspect ratio due to agglomeration in the cured composite material. For the XG-C-THF modified epoxy, the modifiers were more particulate-like, i.e. not platelet-like, and were not as effective at such low volume fractions.

For the GNPs which were first dispersed in NMP, the predicted values of G_C are compared to the experimentally measured values in Figure 25. The XG-H-NMP and GS-NMP modified epoxies show good agreement with the models when all three contributions were accounted for. It was also noted that the contributions from the debonding and pull-out toughening mechanisms were significantly higher than the void growth component for the larger platelets.

The XG-M-NMP and XG-C-NMP modified epoxies show poor agreement

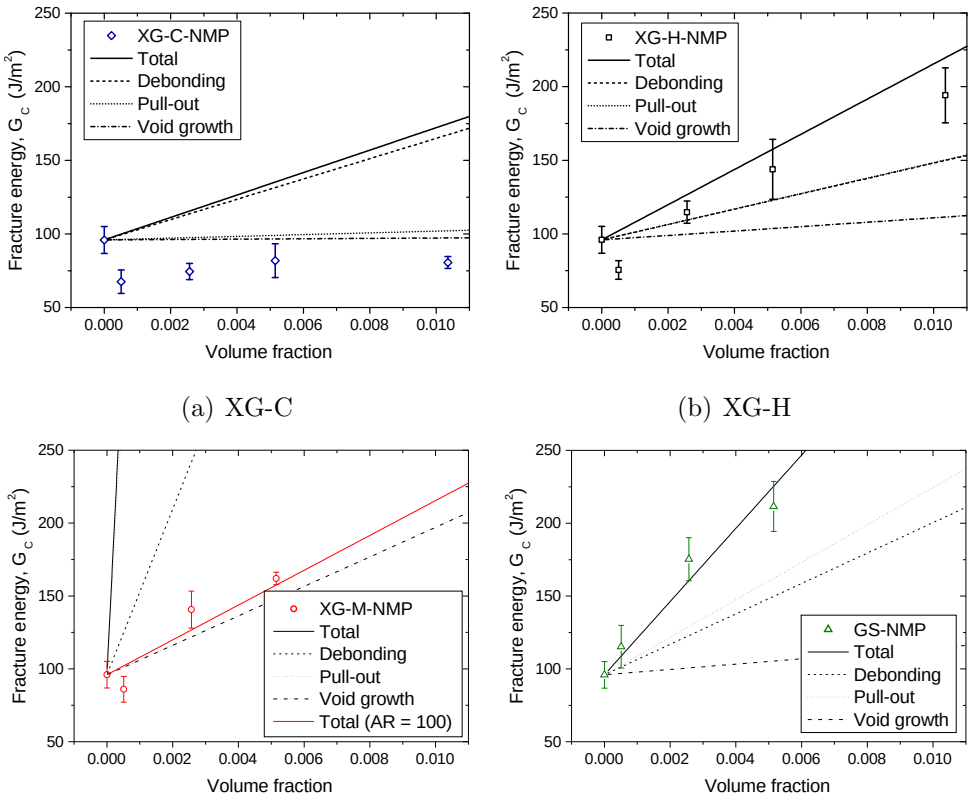

(a) XG-C (b) XG-H

(c) XG-M (d) GS

Figure 25: Predicted (debonding, pull-out and void growth) and measured values of fracture energy for epoxy polymers modified with GNPs dispersed in NMP.

with the model. For the XG-M GNPs, the measured values of G_c show good agreement with only the void growth component of the model. This could either be the result of void growth being the only significant process, in which case it suggests very poorly bonded platelets. However, it is more likely that this is the result of agglomeration resulting in a lower effective aspect ratio. Indeed, when using an aspect ratio of 100 as shown by the red line in Figure 25(c), a good agreement between the model and experimental results was

found. The void growth and debonding mechanisms are directly proportional to the aspect ratio, thus the pull-out mechanism is most likely to be overpredicted as the fracture energy contribution for pull-out is proportional to the debonded length squared, which itself is dependent on the aspect ratio. For the XG-C GNPs, it would appear that the pull-out and void growth mechanisms have insignificant energy contributions, compared to debonding due to the small lateral lengths of the XG-C GNPs. However, as debonding was not observed from the fracture surfaces, the fracture performance was not improved by the addition of the XG-C GNPs. Indeed the observed reduction in G_c indicates that the XG-C GNPs do not act as coherent agglomerates, but, act as defects as has been observed with some other nanoscale particles [58].

5. Conclusions

The influence of the size, aspect ratio, surface functionality and dispersion of several types of graphene nanoplatelets on the mechanical properties of a brittle epoxy polymer were investigated. The composites were manufactured by sonicating the GNPs in solvent (tetrahydrofuran or n-methylpyrrolidone), followed by the addition of epoxy resin and subsequent removal of the solvent. This is the first work to compare a wide range of graphene nanoplatelets, thereby assessing the effects of aspect ratio and functionality, and to quantitatively predict the toughness of the modified epoxies.

The dispersion of the GNPs in the epoxy was examined from the fracture surfaces and varied with platelet size, concentration and type of solvent used. The mechanical properties of the GNP modified epoxies were highly

dependent on the platelet size and aspect ratio. Overall, the highest tensile and fracture properties were measured for the GNPs with intermediate lateral size, namely the GS GNP, due to poor dispersion for the largest platelet size examined. The Young's modulus increased from 2.9 GPa to 3.6 GPa with 1.0 wt% of GS GNPs, when dispersed in NMP. The maximum value of fracture energy was measured for the 2.0 wt% GS GNP modified epoxy, dispersed in THF, at 343 J/m^2. This is an increase of 240% from 96 J/m^2 for the unmodified epoxy. These values will translate to similar increased interlaminar fracture energies for fibre composites. Analysis of the fracture surfaces reveal different toughening mechanisms for the GNPs sonicated in each solvent. When dispersed in THF, the GNPs formed large agglomerates in the cured epoxy, which allows crack deflection to occur as a major toughening mechanism. For the GNPs dispersed in NMP, platelet debonding, pull-out and void growth of the epoxy were observed around the finer GNP structures. Furthermore, the surface modified GNPs showed low fracture toughness due to the lack of debonding, which suppressed the potential toughening mechanisms of pullout and plastic void growth, and their small size limited the crack deflection.

The value of Young's modulus measured was compared to the Halpin-Tsai and Mori-Tanaka models. The values of Young's modulus for the better dispersed GNPs (XG-H-NMP and GS-NMP) agree well with the Halpin-Tsai "random" model as the actual materials represent a similar morphology to that being modelled. The other GNP modified epoxies did not show good agreement due to the significant agglomeration. The fracture energies were also modelled based on the physically observed mechanisms. For the GNPs

dispersed in THF, the crack deflection predictions using the Faber and Evans model show good agreement with the agglomerated GNP modified epoxies sonicated in THF, with the exception of the most heavily agglomerated XG-M where the effective aspect ratio was reduced. For the GNPs dispersed in NMP, the predictive models agree well with the experimental results when all three mechanisms (of debonding, pull-out and void growth) were accounted for. The exceptions are the XG-C and XG-M modified epoxies where platelet agglomeration reduces the effectiveness of the toughening mechanisms. The use of GNPs enables a balance of reinforcement and toughness that cannot be achieved using other conductive modifiers at these low concentrations. This points towards a viable route for the development of new multifunctional thermoset polymers for adhesives and for the matrices of fibre composites for aerospace and automotive applications.

6. Acknowledgements

The authors gratefully acknowledge the award of a PhD scholarship for Dr. H. M. Chong from the Department of Mechanical Engineering at Imperial College London. The authors would like to thank Evonik Hanse (Dr. S. Sprenger) and Haydale (Mr. I. Walters) for the supply of materials, Ms. P. Carry of the Department of Chemical Engineering for her help with the particle size analysis and Mr. R. Sweeney of the Department of Materials for his help with the X-ray diffraction.

References

[1] R. Bagheri, B. T. Marouf, and R. A. Pearson. Rubber-toughened epoxies: A critical review. *Polymer Reviews*, 49(3):201–225, 2009. doi: 10.1080/15583720903048227.

[2] S. Sprenger. Epoxy resins modified with elastomers and surface-modified silica nanoparticles. *Polymer*, 54(18):4790–4797, 2013. doi: 10.1016/j.polymer.2013.06.011.

[3] H. Kim, Y. Miura, and C. W. Macosko. Graphene/polyurethane nanocomposites for improved gas barrier and electrical conductivity. *Chemistry of Materials*, 22(11):3441–3450, 2010. doi: 10.1021/cm100477v.

[4] D. Vuluga, J. M. Thomassin, I. Molenberg, I. Huynen, B. Gilbert, C. Jerome, M. Alexandre, and C. Detrembleur. Straightforward synthesis of conductive graphene/polymer nanocomposites from graphite oxide. *Chemical Communications*, 47(9):2544–2546, 2011. doi: 10.1039/C0CC04623J.

[5] R. J. Young, I. A. Kinloch, L. Gong, and K. S. Novoselov. The mechanics of graphene nanocomposites: A review. *Composites Science and Technology*, 72(12):1459–1476, 2012. doi: 10.1016/j.compscitech.2012.05.005.

[6] J. R. Potts, D. R. Dreyer, C. W. Bielawski, and R. S. Ruoff. Graphene-based polymer nanocomposites. *Polymer*, 52(1):5–25, 2011. doi: 10.1016/j.polymer.2010.11.042.

[7] D. R. Bortz, E. G. Heras, and I. Martin-Gullon. Impressive fatigue life and fracture toughness improvements in graphene oxide/epoxy composites. *Macromolecules*, 45(1):238–245, 2011. doi: 10.1021/ma201563k.

[8] C. Bao, Y. Guo, L. Song, Y. Kan, X. Qian, and Y. Hu. In situ preparation of functionalized graphene oxide/epoxy nanocomposites with effective reinforcements. *Journal of Materials Chemistry*, 21(35):13290, 2011. doi: 10.1039/C1JM11434D.

[9] Q. Liu, X. Zhou, X. Fan, C. Zhu, X. Yao, and Z. Liu. Mechanical and thermal properties of epoxy resin nanocomposites reinforced with graphene oxide. *Polymer-Plastics Technology and Engineering*, 51(3): 251–256, 2012. doi: 10.1080/03602559.2011.625381.

[10] L. Ramos-Galicia, L. N. Mendez, A. L. Martnez-Hernndez, A. Espindola-Gonzalez, I. R. Galindo-Esquivel, R. Fuentes-Ramirez, and C. Velasco-Santos. Improved performance of an epoxy matrix as a result of combining graphene oxide and reduced graphene. *International Journal of Polymer Science*, 2013:1–7, 2013. doi: 10.1155/2013/493147.

[11] H. Kim, A. A. Abdala, and C. W. Macosko. Graphene/polymer nanocomposites. *Macromolecules*, 43(16):6515–6530, 2010. doi: 10.1021/ma100572e.

[12] S. Chatterjee, F. Nafezarefi, N. H. Tai, L. Schlagenhauf, F. A. Nesch, and B. T. T. Chu. Size and synergy effects of nanofiller hybrids including graphene nanoplatelets and carbon nanotubes in mechanical

properties of epoxy composites. *Carbon*, 50(15):5380–5386, 2012. doi: 10.1016/j.carbon.2012.07.021.

[13] M. A. Rafiee, J. Rafiee, Z. Wang, H. Song, Z. Z. Yu, and N. Koratkar. Enhanced mechanical properties of nanocomposites at low graphene content. *ACS Nano*, 3(12):3884–3890, 2009. doi: 10.1021/nn9010472.

[14] I. Zaman, T. T. Phan, H.-C. Kuan, Q. Meng, L. T. B. La, L. Luong, O. Youssf, and J. Ma. Epoxy/graphene platelets nanocomposites with two levels of interface strength. *Polymer*, 52(7):1603–1611, 2011. doi: 10.1016/j.polymer.2011.02.003.

[15] I. Zaman, H. C. Kuan, J. Dai, N. Kawashima, A. Michelmore, A. Sovi, S. Dong, L. Luong, and J. Ma. From carbon nanotubes and silicate layers to graphene platelets for polymer nanocomposites. *Nanoscale*, 4 (15):4578–86, 2012. doi: 10.1039/c2nr30837a.

[16] Haydale Ltd. *HDPlas™ GNP-COOH Technical data sheet. Haydale Ltd, Carmarthenshire.* 2013.

[17] Haydale Ltd. *HDPlas™ GNP-O_2 Technical data sheet. Haydale Ltd, Carmarthenshire.* 2013.

[18] XG Sciences. *xGnP Grade C product characteristics. XG Sciences, Lansing.* 2013.

[19] XG Sciences. *xGnP Grade H product characteristics. XG Sciences, Lansing.* 2013.

[20] XG Sciences. *xGnP Grade M product characteristics. XG Sciences, Lansing.* 2013.

[21] Graphene Supermarket. Graphene Nanopowder: 12 nm Flakes-25 g. [Online]. *Available from:* *https://graphene-supermarket.com/Graphene-Nanopowder-12-nm-Flakes-5-g-SKU-NP* [Accessed 23rd June 2014].

[22] L. T. Drzal. Graphite nanoreinforcements for aerospace nanocomposites. *Final Report for NASA Langley Research Center, NAG1-01004*, 2005.

[23] P. Scherrer. Bestimmung der grösse und der inneren struktur von kolloidteilchen mittels röntgenstrahlen. *Nachrichten von der Gesellschaft der Wissenschaften zu Göttingen, Mathematisch-Physikalische Klasse*, 26:98–100, 1918.

[24] J. F. Watts and J. Wolstenholme. *An Introduction to Surface Analysis by XPS and AES.* John Wiley & Sons, New York, 2003. doi: 10.1002/0470867930.

[25] ISO 527-2. *Plastics - Determination of tensile properties - Part 2: Test conditions for moulding and extrusion plastics.* International Standards Organisation: Geneva, 1996.

[26] J. G. Williams and H. Ford. Stress-strain relationships for some unreinforced plastics. *Journal of Mechanical Engineering Science*, 6(4): 405–417, 1964. doi: 10.1243/JMES_JOUR_1964_006_055_02.

[27] P. B. Bowden and S. Raha. The formation of micro shear bands in

polystyrene and polymethylmethacrylate. *Philosophical Magazine*, 22 (177):463–482, 1970. doi: 10.1080/14786437008225837.

[28] Y. Huang and A. J. Kinloch. Modelling of the toughening mechanisms in rubber-modified epoxy polymers. Part II. A quantitative description of the microstructure-fracture property relationships. *Journal of Materials Science*, 27:2763–2769, 1992. doi: 10.1007/BF00540703.

[29] J. N. Sultan and F. J. McGarry. Effect of rubber particle size on deformation mechanisms in glassy epoxy. *Polymer Engineering & Science*, 13(1):29–34, 1973. doi: 10.1002/pen.760130105.

[30] ISO 13586. *Plastics - Determination of fracture toughness (G_{IC} and K_{IC}) - Linear elastic fracture mechanics (LEFM) approach.* International Standards Organisation: Geneva, 2000.

[31] J. S. Lukesh and L. Pauling. The problem of the graphite structure. *American Mineralogist*, 35:125, 1950.

[32] V. V. Ivanovskaya, P. Wagner, A. Zobelli, I. Suarez-Martinez, A. Yaya, and C. P. Ewels. *Graphene Edge Structures: Folding, Scrolling, Tubing, Rippling and Twisting*, chapter 10, pages 75–85. Carbon Nanostructures. Springer Berlin Heidelberg, 2012. doi: 10.1007/978-3-642-20644-3_10.

[33] G. Beamson and D. Briggs. *High Resolution XPS of Organic Polymers: The Scienta ESCA300 Database.* John Wiley & Sons, New York, 1992. doi: 10.1021/ed070pA25.5.

[34] A. J. Kinloch and A. C. Taylor. The mechanical properties and fracture behaviour of epoxy-inorganic micro- and nano-composites. *Journal of*

Materials Science, 41(11):3271–3297, 2006. doi: 10.1007/s10853-005-5472-0.

[35] R. J. Zaldivar, J. P. Nokes, P. M. Adams, K. Hammoud, and H. I. Kim. Surface functionalization without lattice degradation of highly crystalline nanoscaled carbon materials using a carbon monoxide atmospheric plasma treatment. *Carbon*, 50(8):2966–2975, 2012. doi: 10.1016/j.carbon.2012.02.079.

[36] G. Tillet, B. Boutevin, and B. Ameduri. Chemical reactions of polymer crosslinking and post-crosslinking at room and medium temperature. *Progress in Polymer Science*, 36(2):191–217, 2011. doi: 10.1016/j.progpolymsci.2010.08.003.

[37] C. Lee, X. Wei, J. W. Kysar, and J. Hone. Measurement of the elastic properties and intrinsic strength of monolayer graphene. *Science*, 321 (5887):385–8, 2008. doi: 10.1126/science.1157996.

[38] E. H. Andrews. *Fracture in Polymers*. Oliver & Boyd, Edinburgh, 1968.

[39] K. T. Faber and A. G. Evans. Crack deflection processes I. Theory. *Acta Metallurgica*, 31(4):565–576, 1983. doi: 10.1016/0001-6160(83)90046-9.

[40] T. H. Hsieh, A. J. Kinloch, K. Masania, J. Sohn Lee, A. C. Taylor, and S. Sprenger. The toughness of epoxy polymers and fibre composites modified with rubber microparticles and silica nanoparticles. *Journal of Materials Science*, 45(5):1193–1210, 2010. doi: 10.1007/s10853-009-4064-9.

[41] X. L. Gao and K. Li. A shear-lag model for carbon nanotube-reinforced polymer composites. *International Journal of Solids and Structures*, 42 (5-6):1649–1667, 2005. doi: 10.1016/j.ijsolstr.2004.08.020.

[42] Y. Hernandez, V. Nicolosi, M. Lotya, F. M. Blighe, Z. Sun, S. De, I. T. McGovern, B. Holland, M. Byrne, Y. K. Gun'Ko, J. J. Boland, P. Niraj, G. Duesberg, S. Krishnamurthy, R. Goodhue, J. Hutchison, V. Scardaci, A. C. Ferrari, and J. N. Coleman. High-yield production of graphene by liquid-phase exfoliation of graphite. *Nature Nanotechnology*, 3(9): 563–568, 2008. doi: 10.1038/nnano.2008.215.

[43] W. Zhao, F. Wu, H. Wu, and G. Chen. Preparation of colloidal dispersions of graphene sheets in organic solvents by using ball milling. *Journal of Nanomaterials*, 2010(528325):1–5, 2010. doi: 10.1155/2010/528235.

[44] R. A. Pearson and A. F. Yee. Influence of particle size and particle size distribution on toughening mechanisms in rubber-modified epoxies. *Journal of Materials Science*, 26(14):3828–3844, 1991. doi: 10.1007/BF01184979.

[45] F. J. Guild, A. J. Kinloch, and A. C. Taylor. Particle cavitation in rubber toughened epoxies: the role of particle size. *Journal of Materials Science*, 45(14):3882–3894, 2010. doi: 10.1007/s10853-010-4447-y.

[46] Y. Lee, S. Bae, H. Jang, S. Jang, S.-E. Zhu, S. H. Sim, Y. I. Song, B. H. Hong, and J.-H. Ahn. Wafer-scale synthesis and transfer of graphene films. *Nano Letters*, 10(2):490–493, 2010. doi: 10.1021/nl903272n.

[47] T. Herceg, M. S. Z. Abidin, C. Delfour, E. Greenhalgh, A. Bismarck, and M. Shaffer. Scalable production of epoxy based nanocomposites and hierarchical composites with high CNT loadings. *19th International Conference on Composite Materials, 28 July-2 August 2013, Montreal, Canada*, 2013.

[48] J. C. Halpin and N. J. Pagano. The laminate approximation for randomly oriented fibrous composites. *Journal of Composite Materials*, 3 (4):720–724, 1969. doi: 10.1177/002199836900300416.

[49] J. C. Halpin and J. L. Kardos. The Halpin-Tsai equations: A review. *Polymer Engineering & Science*, 16(5):344–352, 1976. doi: 10.1002/pen.760160512.

[50] M. A. Van Es. Polymer-clay nanocomposites: the importance of particle dimensions. *PhD Thesis, Faculty of Applied Sciences, Delft University of Technology*, 2001.

[51] T. Mori and K. Tanaka. Average stress in matrix and average elastic energy of materials with misfitting inclusions. *Acta Metallurgica*, 21(5): 571–574, 1973. doi: 10.1016/0001-6160(73)90064-3.

[52] G. P. Tandon and G. J. Weng. The effect of aspect ratio of inclusions on the elastic properties of unidireectionally aligned composites. *Polymer Composites*, 5(4):327–333, 1984. doi: 10.1002/pc.750050413.

[53] T. H. Hsieh, A. J. Kinloch, A. C. Taylor, and I. A. Kinloch. The effect of carbon nanotubes on the fracture toughness and fatigue performance

of a thermosetting epoxy polymer. *Journal of Materials Science*, 46(23): 7525–7535, 2011. doi: 10.1007/s10853-011-5724-0.

[54] D. J. Green, P. S. Nicholson, and J. D. Embury. Fracture of a brittle particulate composite. Part 1. Experimental aspects. *Journal of Materials Science*, 14(6):1413–1420, 1979. doi: 10.1016/0010-4361(79)90034-X.

[55] B. B. Johnsen, A. J. Kinloch, R. D. Mohammed, A. C. Taylor, and S. Sprenger. Toughening mechanisms of nanoparticle-modified epoxy polymers. *Polymer*, 48(2):530–541, 2007. doi: 10.1016/j.polymer.2006.11.038.

[56] D. Hull and T.W. Clyne. *An Introduction to Composite Materials*. Cambridge University Press, Cambridge, 1981.

[57] A. H. Barber, S. R. Cohen, S. Kenig, and H. D. Wagner. Interfacial fracture energy measurements for multi-walled carbon nanotubes pulled from a polymer matrix. *Composites Science and Technology*, 64(15): 2283–2289, 2004. doi: 10.1016/j.compscitech.2004.01.023.

[58] A. J. Kinloch and A. C. Taylor. The toughening of cyanate-ester polymers. Part I Physical modification using particles, fibres and woven-mats. *Journal of Materials Science*, 37(3):433–460, 2002. doi: 10.1023/A:1013735103120.